Master's Thesis

Torque Model for Position Control of Multi-degree of Freedom Electromagnetic Actuator

Sang-A Park

Department of Mechanical Engineering

Graduate School of UNIST

2017

Torque Model for Position Control of Multi-degree of Freedom Electromagnetic Actuator

Sang-A Park

Department of Mechanical Engineering

Graduate School of UNIST

Torque Model for Position Control of Multi-degree of Freedom Electromagnetic Actuator
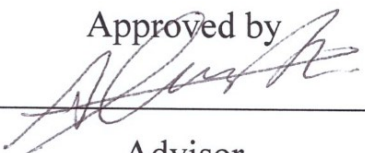
A thesis

submitted to the Graduate School of UNIST

in partial fulfillment of the

requirements for the degree of

Master of Science

Sang-A Park

1. 19. 2017

Approved by

_____

Advisor

Hungsun son

Torque Model for Position Control of Multi-degree of Freedom Electromagnetic Actuator

Sang-A Park

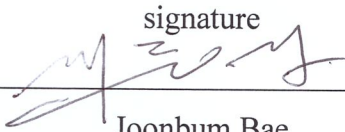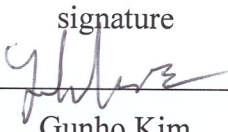This certifies that the thesis of Sang-A Park is approved.

1.19.2017

signature

Advisor: Hungsun Son

signature

Joonbum Bae

signature

Gunho Kim

Abstract

A Spherical Wheel Motor (SWM) is one of electromagnetic actuators capable of providing three degree of freedom (DOF) rotational motions as a single device. The SWM can be applied to many application such as industrial robots, humanoid robots, surgical instrument, etc due to its compactness. However, the existed SWM has to be improved to apply practical applications in the areas of compact design, force and torque, and control systems and so on.

The objective of the thesis is to develop the method of torque model for SWM and position control using in open loop control. The torque model requires understanding the design of SWM as well as magnetic fields analysis. In particular, the analysis of magnetic fields of the SWM is very difficult and requires long computational time due to complexity and a number of magnetic poles. The existing models based on numerical methods may not be suitable to control the SWM. Therefore, the simple but accurate torque model is required to real-time control. In previous research, the torque model of SWM was demonstrated the summation of interaction between each permanent magnets and electromagnets as the magnetic circuit is linear. In this work, the equations of interaction between the permanent magnets and electromagnets was simplified using the structural characteristic of SWM. The torque model was suggested in closed-form using simplified torque model. The experiment and other simulations were performed to check the validity of simplified torque model. To verify the simplified torque model, the position control was operated using push-pull principal. To demonstrate that the torque model and position control principal were proper, the experiment was performed the position control in open-loop control.

The simplified torque model offers fast computational performance compared with other simulation tools results, and shows that the torque values are reasonable to control. Furthermore, the experiment results show that the SWM is properly controlled the position using the proposed torque model and position control mechanism.

Contents

List of Figure

List of Table

Nomenclature

Symbol	Description	Unit
$R_{r,i}, R_{r,o}$	Radius of inner and outer rotor	mm
$R_{PM,i}, R_{PM,o}$	Radius of PM at inner and outer rotor respectively	mm
$h_{PM,i}, h_{PM,o}$	Height of PM at inner and outer rotor respectively	mm
R_{core}	Radius of EM core	mm
$R_{coil,in}, R_{coil,out}$	Radius of coils which located at inside and outside in stator plate	mm
$h_{coil,in}, h_{coil,out}$	Height of inner and outer coil	mm
$\beta_r,$	Angle between the PMs in column	°(degree)
δ_r	Angle between the PMs in row	°(degree)
β_s	Angle between the EM and *XY*-plane	°(degree)
δ_s	Angle between the EM in row	°(degree)
r	The position vector of rotor	
s	The position vector of stator	
$[L]$	Inductance Matrix	
u_r	Polarity Matrix of the rotor	
u_s	Stator current input vector	A
$T_{x,y,z}$	Torque vector in *xyz*-coordinate frame	N/mm
q	Orientation Vector in spherical coordinate	rad
T_{jk}	Torque as a result of the interaction j^{th} EM with k^{th} PM	N/mm
$T_{\Delta j}$	The simplified torque term which is generated by j^{th} EM	N/mm
φ_{jk}	The separation angle between j^{th} stator pole pair with k^{th} rotor	rad
f	An approximate torque magnitude function	
n_s, n_r	The number of poles of stator and rotor	

$\omega_1, \omega_2, \omega_3$	The orientation angle in Z-y`-z coordinate frame	
$[\Gamma]$	The coordinate transformation matrix	
B	the magnetic flux density (MFD)	T
F	Lorentz force	N

I. Introduction

The conventional motors only offer single axis rotation. Generally, the typical motion manipulators need a tool which has several single-axis rotation motors such as serial manipulator, parallel manipulator to control multi-degree of freedom. Industrial robot is an example of the serial manipulators, and Stewart Motion Platform is an example of the parallel manipulator as shown in **Fig 1.1**. These kinds of manipulators have problems that they need additional power transfer systems, singularity problems, and so on. In addition, they have the low accuracy problems caused by the mechanical friction and backlash.

(a)   (b)
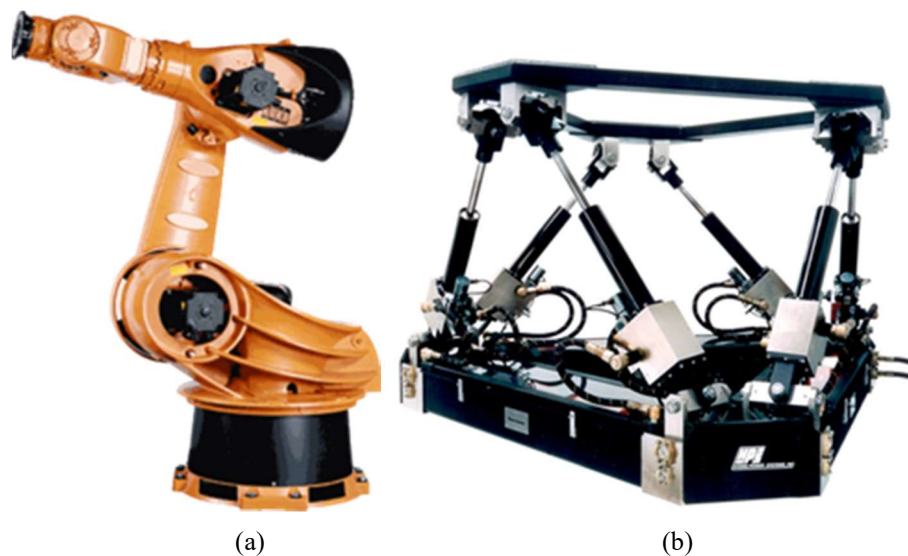
Fig.1.1 Examples of Multi-Degree of Freedom Manipulators (a) 6DOF Serial Manipulator (KUKA Robotics Corporation) (b) 6DOF Parallel Manipulator (Hydra Power System)

Spherical motor is one of the special actuators which are developed to improve the problems mentioned above. It can be driven by simultaneous three-dimensional rotation. It has several advantages: weight loss and improved energy efficiency and accuracy according to the minimized number of motors and components. Besides, the spherical motor can solve the kinematic singularity problems. The spherical motor is developed in various types, a spherical motor that takes a number of forms including the stepper [1], induction motor [2] [3], direct-current motor [4] [5] [6], variable-reluctance motor [7] [8] [9], ultrasonic motor [10]. Recently, remarkable two types of spherical motors are developed. One is ultrasonic spherical motor [10], the other is spherical wheel motor (SWM) [11]. The ultrasonic spherical motor comes from the extension of the typical single-axis ultrasonic motors which use two natural vibrations of the stator to drive the rotor with frictional force. The principle of SWM is based on the conventional single-axis motor. **Table 1.1** shows the characteristics of the two types. Especially, SWM has several benefits inherited from the conventional electromagnetic motors and corresponding

control strategies. From these reason, the development of SWM is required.
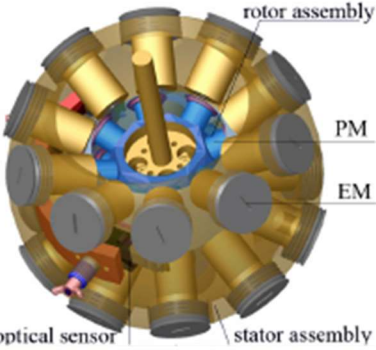
	Ultrasonic Spherical Motor	Spherical Wheel Motor
Comparison	-Compact size -Simple structure -High torque density -Complicate manufacturing process -Require high voltage and frequency	-Advantage of conventional electromagnetic motors -Correspond control strategies with conventional electromagnetic motors

Table 1.1 Comparison of Ultrasonic Spherical Motor and Spherical Wheel Motor

There are many research subject for the SWM. Among them, the magnetic field analysis is an indispensable research subject in SWM control for torque calculation. Existing techniques for analyzing electromagnetic fields are analytic solutions to Laplace equation, numerical methods and several computational methods such as lumped-parameter analysis and so on. The analytical and numerical methods are based on Maxwell equations with boundary conditions. But analytical methods are limited and hard to solve. Numerical methods shows good accuracy but they have computational cost problems. So many researchers are using several other computation methods such as finite element, boundary element finite difference and mesh free methods and so on. These methods offer a good prediction of the magnetic fields for accurate computation of the magnetic torque. However, these approaches have difficulties in achieving both accuracy and short computation time for efficient design and robust control of the actuators. So they are still not proper tools for the real-time control which requires the higher accuracy and the less computation time. Here in, we propose a new approach to calculate torque for the real-time control.

The basic concept of this approach is that the torque equation can be expressed by interaction between the permanent magnets and electromagnets. The torque model is suggested in the closed-form using simplified torque model. The experiment and other simulations are performed to verify the validity of the simplified torque model. For that, the position control is operated by using push-pull principle. The position control experiment is operated in open-loop control.

II. Design of Spherical Wheel Motor

The basic principle of electromagnetic actuator is based on interactions between permanent magnets (PM) and electromagnets (EM). For SWMs which use this principle, the arrangement of PMs and EMs is also important. Previously researchers studied the design of SWMs which have the arrangement that showed maximized torque force. In this chapter, an explanation of the arrangement of permanent magnets and electromagnets and the shape of electromagnets is presented. The design of the SWM is shown in the **Figure 2.1**, and the design parameters of SWM are as shown in the **Table 2.1**.
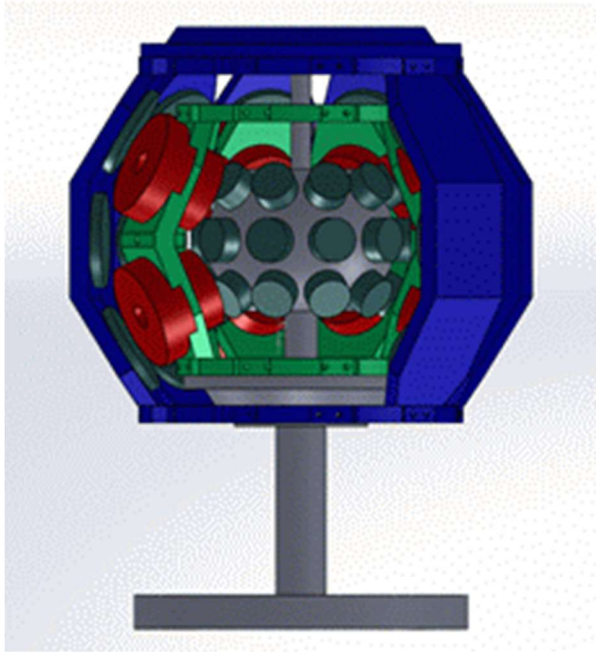
Fig.2.1 The design of SWM

Rotor		Stator	
$R_{r,i}$	25mm	R_s	45mm
$R_{r,o}$	58mm	R_{core}	3.75mm
$R_{PM,i}$	6.5mm	$R_{coil,in}$	12mm
$h_{PM,i}$	8mm	h_{in}	10.5mm
$R_{PM,o}$	14mm	$R_{coil,out}$	16mm
$h_{PM,o}$	6mm	h_{out}	10.5mm
β_r	32°	β_s	24°
δ_r	36°	δ_s	45°

Table 2.1 The design parameter of SWM

The subscripts "r" and "s" denotes the rotor and stator, respectively. Also, "R" and "h" denotes the radius and height of the cylinder, respectively. $R_{r,i}$ and $R_{r,o}$ are the distances from the center of the ball bearing to the surface of the nearest inner and outer permanent magnets. R_s is a distance from the center of ball bearing to surface between two coil which composes one electromagnet. The brief explanation of the notations is in the Nomenclature section.

2.1 Arrangement of the Permanent Magnets and Electromagnets

The most important design parameter is the arrangement of PMs and EMs. The arrangement at home position is shown in **Fig 2.1**. It represents each coordinate systems fixed at rotor and stator. The rotor have 30 pairs of PMs – three layers of ten PM pairs each; one pair of PM means PM at inner rotor and PM at outer rotor. The PM pair are installed aligned to the center of rotor with the same polarity direction. The PMs have the opposite polarity between neighboring PMs. In other words, the polarity of PMs can be represented $u_i = -u_{i+1}$ and $u_1 = +1$. The ten pairs are arranged radial-circularly as shown in **Fig 2.1.1 (a)**. The angle between the two neighboring poles on the circumference is δ_r (36 degrees). The angle between the plane of rotor poles and the *XY*-plane is β_r. There are three planes of rotor poles: One plane is located at *XY*-plane and others are located with the separation angle (β_r) between *XY*-plane as shown **Fig 2.1.1 (b)**. Position vector of PMs of rotor at home position are given by:

$$
\begin{aligned}
r_{3(i-1)+1} &= R_{i,o}\left[\cos\beta_r\cos(i-1)\delta_r \quad \cos\beta_r\sin(i-1)\delta_r \quad \sin\beta_r\right] \\
r_{3(i-1)+2} &= R_{i,o}\left[\cos(i-1)\delta_r \quad \sin(i-1)\delta_r \quad 0\right] \\
r_{3(i-1)+3} &= R_{i,o}\left[\cos\beta_r\cos(i-1)\delta_r \quad \cos\beta_r\sin(i-1)\delta_r \quad -\sin\beta_r\right]
\end{aligned}
\tag{2.1}
$$

where R_i is the distance from center of SWM to inner PM, and R_o is the distance from the center to outer PM. The position vectors are representative at home-position in absolute coordinate which is fixed at stators.

The stator is composed of 16 EMs which are two layers of eight EMs; the shape of EM is described in the *section 2.2*. The 8 EMs are arranged radial-circularly in one layer. Similarly, the angle between two neighboring poles on the circumference EM is δ_r (45 degrees). The two planes of stator poles have an angle β_s between the *XY*-plane as shown in **Fig. 2.1.1 (b)**. Position vectors of EMs of stator in absolute coordinates are given by:

$$
\begin{aligned}
s_{2(i-1)+1} &= R_s\left[\cos\beta_s\cos(i-1)\delta_s \quad \cos\beta_s\sin(i-1)\delta_s \quad \sin\beta_s\right] \\
s_{2(i-1)+2} &= R_s\left[\cos\beta_s\cos(i-1)\delta_s \quad \cos\beta_s\sin(i-1)\delta_s \quad -\sin\beta_s\right]
\end{aligned}
\tag{2.2}
$$

Where R_s is the center-to-center distance between each coil.

(a)   (b)
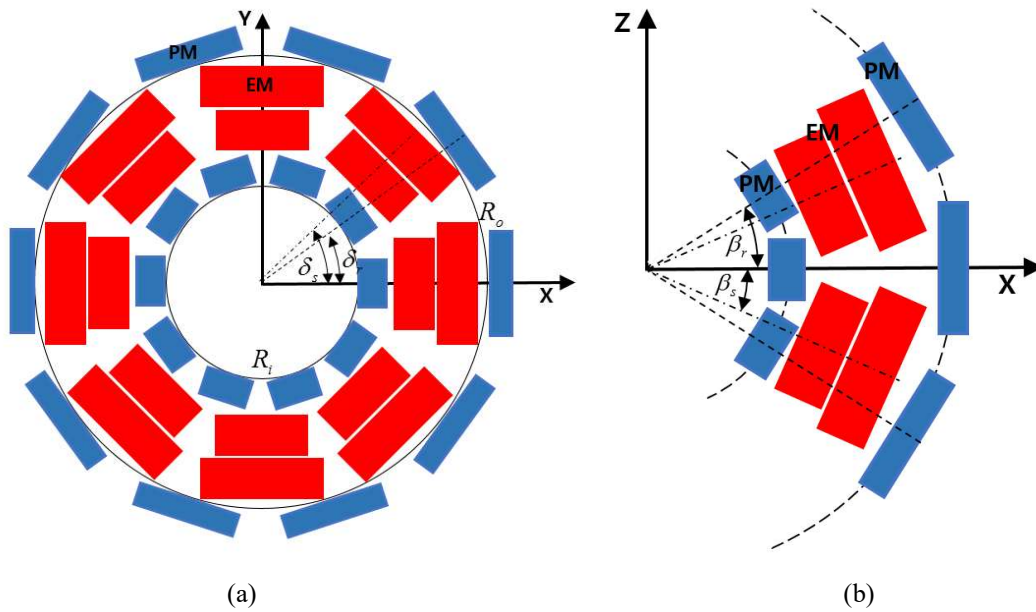
Fig. 2.1.1 The arrangement of PMs and EMs (a) the top-view (b) side cross-section view

The explained position vectors of PMs and EMs follow numbering systems. During this study, the numbering systems of rotor poles and stator poles are decided as shown in **Fig 2.1.2**. The number is increased from top to bottom, and from left side to right side. Furthermore, the $1^{st} \sim 3^{rd}$ PMs are located at right half-plane of xz-plane in body rotor frame and numbering rotation direction is positive z-direction. Similarly, the first two EMs are located at the right half-plane of XZ-plane in absolute frame.

(a)   (b)
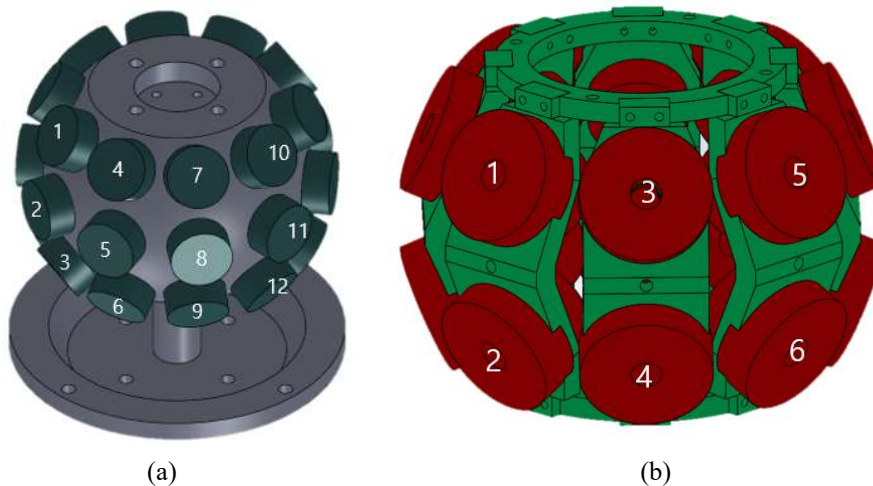
Fig. 2.1.2 Numbering system of rotor poles and stator poles; (a) numbering system of rotor (b) numbering system of stator

2.2 Shape of Electromagnets (Coil)

As shown in the previous section, the design of EM is composed of two coils which represent two different size of cylinder coils. The EM is fastened to the stator plate. For this, the EM has to be composed of two coils which are connected to the core. Three different types of coils are shown in **Fig. 2.2.1**, which is designed to avoid interference between EMs and PMs so to protect the coil damages.
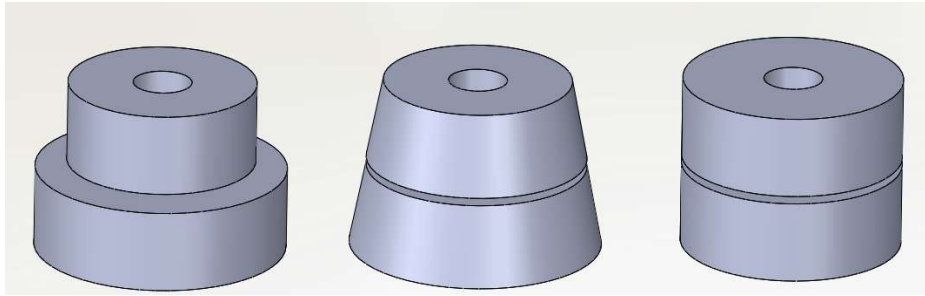
Fig. 2.2.1 The types of coils (a) Type A: Two different size of Cylinders (b) Type B: Taper (c) Type C: Two same size of cylinders.

Type A is composed of two differently sized coils. The radius of small one is 12 mm and the height is 10.5 mm. The radius of the large one is 16 mm and the height is 10.5 mm. Type B is composed of taper-shaped cylinders. The radius of each taper is 16 mm to 14 mm and 14 mm to 12 mm and the height both are 10.5 mm. The type C is composed of two same cylinders. The radius is 14 mm and the height is 10.5 mm. All these designs have the same volume and the number of turns. The wire diameter of coils is 0.4 mm. The core is made with Aluminum and they are assembled by plastic screw.

First, the magnetic fields simulation for each coil is performed by using COMSOL magnetic fields analysis function. **Fig 2.2.2** is the simulation result of Type A, **Fig 2.2.3** is the magnetic field of Type B, and **Fig 2.2.4** shows the result of Type C. The required input values during the simulation are the number of turns, the standard of wire, current, material and so on. The number of turns is calculated with the areas divided by the thickness of the coil (the standard of the wire is 0.4mm, current is 1A and material is copper). The torque is represented next to each simulation result and the unit is T (teslas).
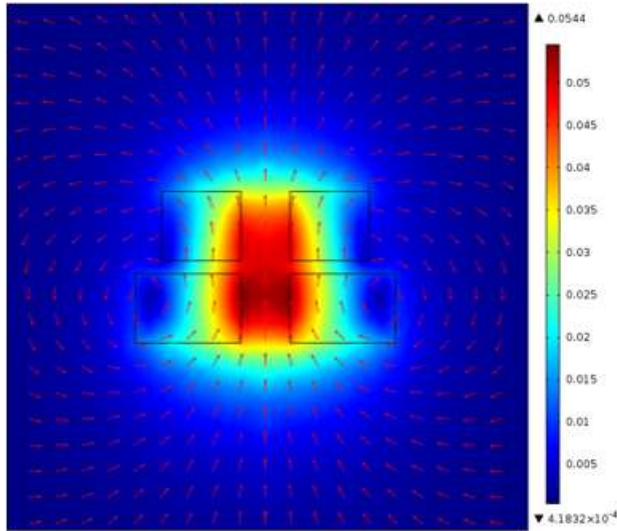
Fig. 2.2.2 The magnetic analysis simulation results of Type A
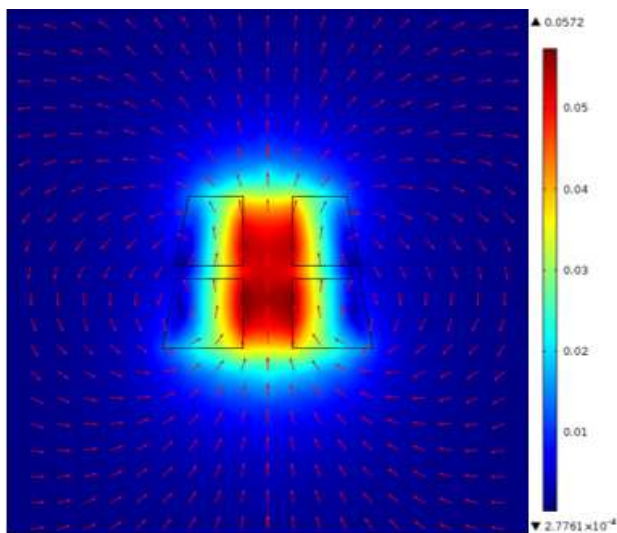
Fig. 2.2.3 The magnetic analysis simulation results of Type A
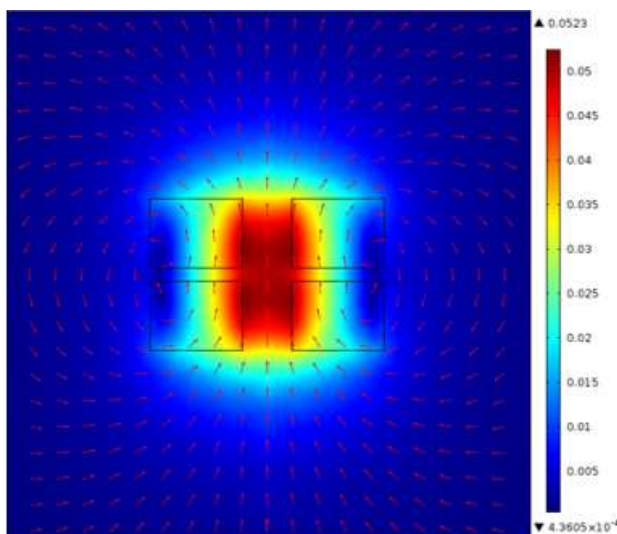
Fig. 2.2.4 The magnetic analysis simulation results of Type C

(a)   (b)
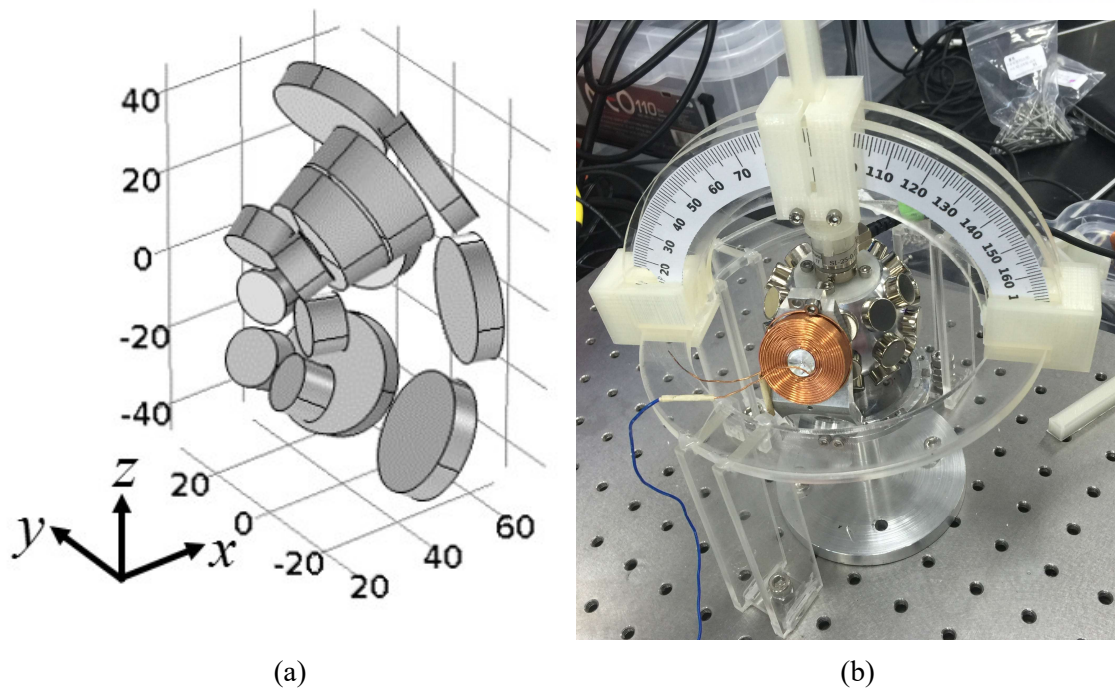
Fig. 2.2.5 Simulation set-up: Home Position; (a) COMSOL simulation structure (b) Experimental set-up

Second, the torque generation simulation is carried out. The COMSOL simulation is set-up by using only one EM and six PM pairs with two columns which are like the arrangement of $1^{st} \sim 6^{th}$ PMs in SWM design as shown in **Fig 2.2.5 (a)**. The two columns of the PMs are located planar to xz-plane of COMSOL frame. The position of EM is along the right half plane of xz-plane which is the center between $1^{st} \sim 3^{rd}$ PMs and $4^{th} \sim 6^{th}$ PMs. **Fig 2.2.5 (a)** shows the home-position of rotors. The rotation angle means y-directional rotation angle, which is related to the separation angle between the plane of EM pole and xy-plane of rotor, and which is subtracted by the home position of rotor; simply, the rotation angle is zero when home-position which is the separate angle is β_r. The experiment set-up is shown in **Fig 2.2.5 (b)**. The angle guide is made with acrylic panel and 3D printer. The torque sensor is located between the rotor and shaft which are fastened to the guide.

There are two cases of simulations: using only inner PM and using PM pairs. The COMSOL simulation result is shown below:

(a)

(b)

(c)

(d)

(e)

(f)
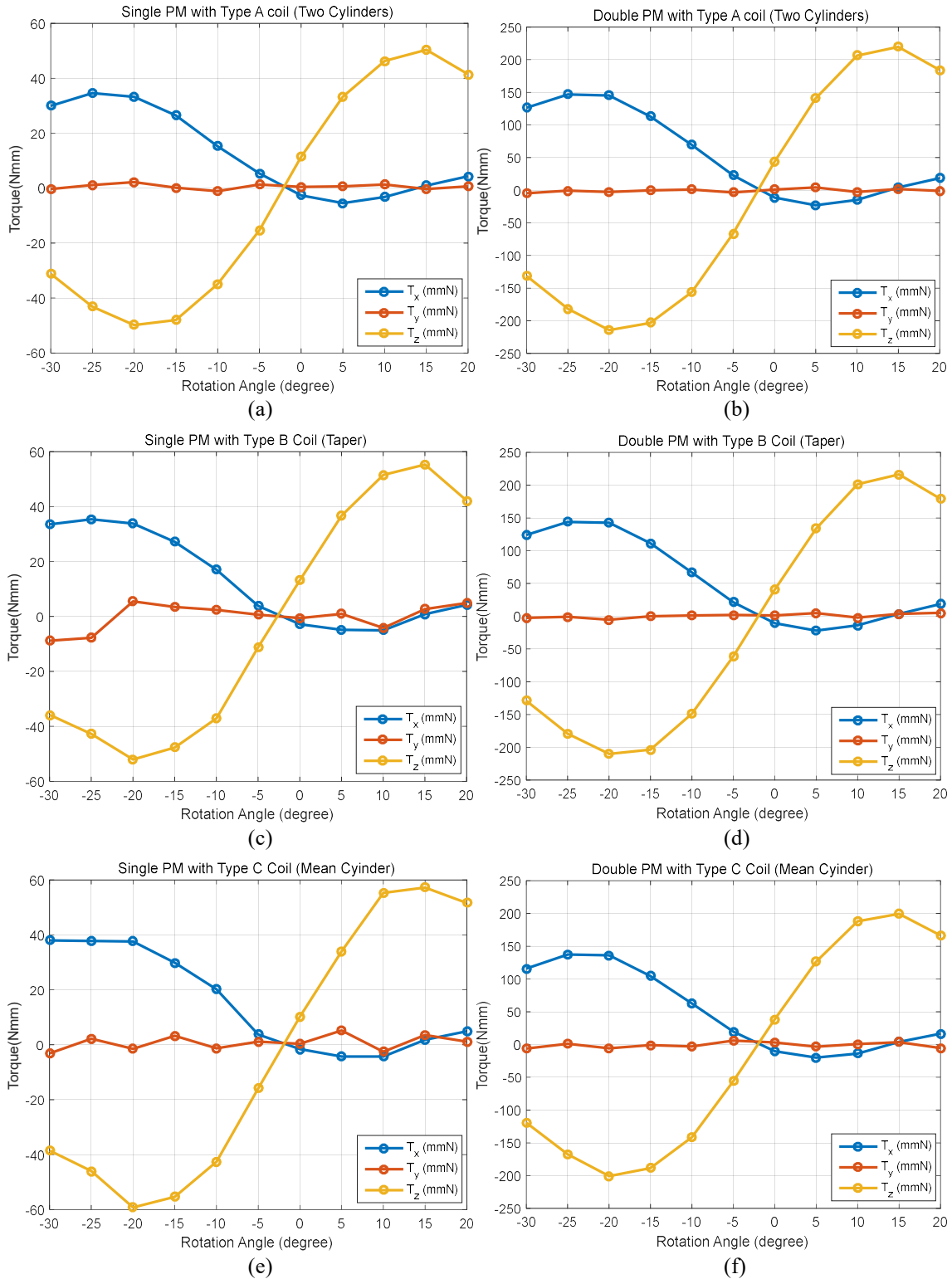
Fig. 2.2.6 The COMSOL simulation results; (a) Type A with Single PM (b) Type A with Double PMs (c) Type B with Single PM (d) Type B with Double PMs (e) Type C with Single PM (f) Type C with Double PMs

The experiment is proceeded with the same set-up. The result graphs are shown below:
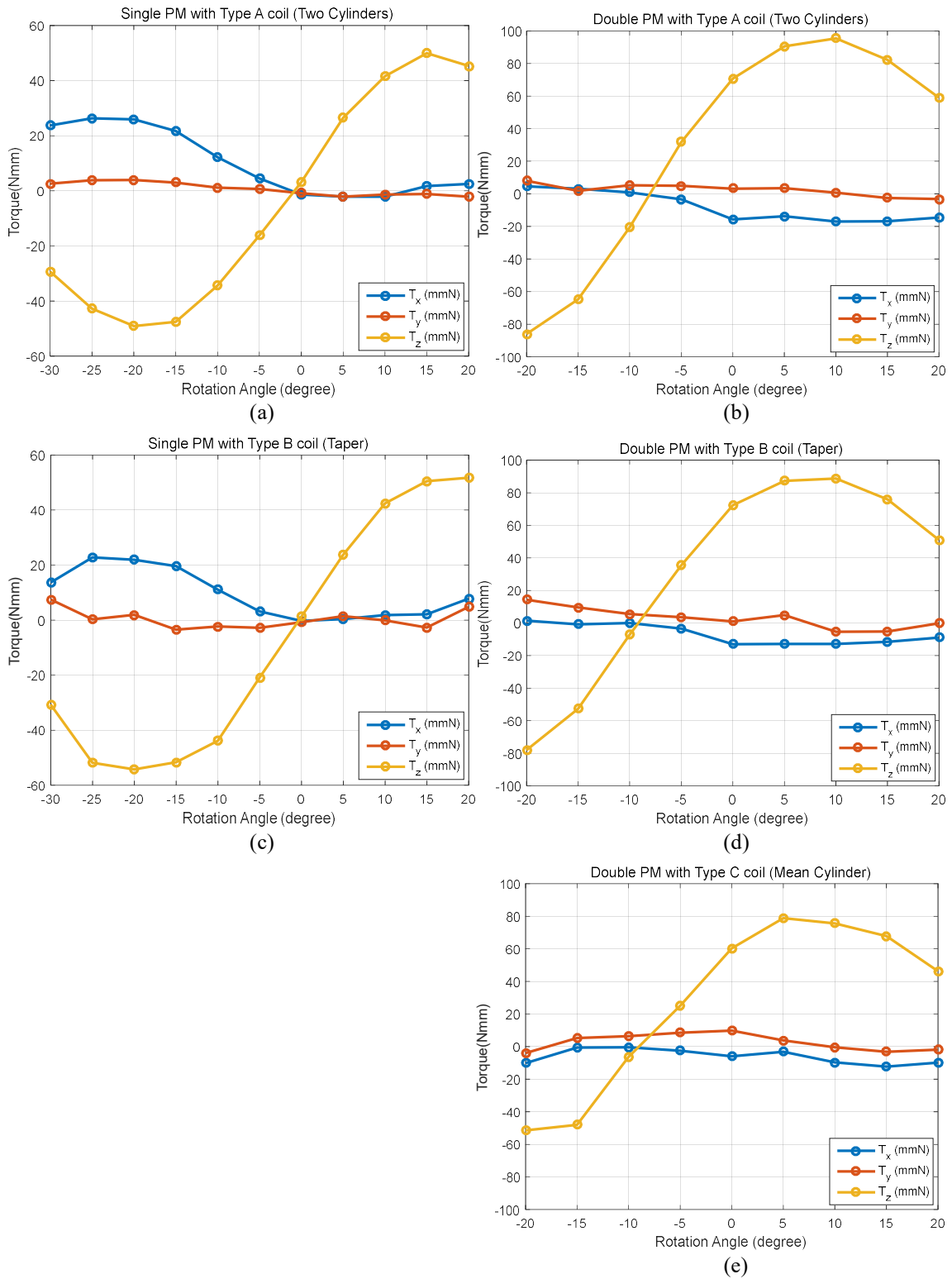
Fig. 2.2.7 The Experiment results; (a) Type A with Single PM (b) Type A with Double PMs (c) Type B with Single PM (d) Type B with Double PMs (e) Type C with Single PM (f) Type C with Double PMs

The COMSOL simulation results are shown at **Fig2.2.6**. First case of the simulation results are the graphs on the first column; single 6 PMs with each type of coil. The second column graphs are the second case; 6 PM pairs with each type of coil. All graphs showed the similar trend. In the first case, the Type C has the largest maximum torque value and the Type A has the smallest torque vale. This result can be explained by the volume of nearest part of coils from the inner PMs. The order of each volume correspond to that of the torque value of the same angles; $V_{TypeC} > V_{TypeB} > V_{TypeA}$. In the second simulation case, the order of maximum torque value is changed: Type A and Type B have similar torque values. To summarize, for the whole SWM design case with COMSOL simulation, Type A and Type B can make larger torque than Type C.

Now **Fig2.2.7** shows the experiment results. It seems similar to the COMSOL simulation result. But there are three differences; the Type C is not used for the first case, the coil current of second case is 0.5 A (the simulation is 1 A), and the rotation angle range is changed.

According to the first column graphs of the simulation results, it is obvious that the Type C have the largest torque value because the diameter of Type C (which is closest to the PM) is different. Therefore, The Type C is excluded. Then the Type B shows the next largest max torque both in the simulation and the experiment. In the second case, the second column graphs show the results. The torque sensor used for the experiment has the sensing range of ±100Nmm. For this reason, the coil current is set to 0.5A. Besides, because each coil have different number of wiring, after-data-processing is done for each result. After the data processing, the experimental results show similar trend with the simulation. Based on that, the coil Type A is chosen; though Type A and Type B show the similar value, the Type A can be easily manufactured than Type B.

III. Torque Model

The torque of spherical motor can be derived by differentiating the magnetic co-energy. [7]:

$$T = \frac{1}{2} u_s^T \frac{\partial [L_{ss}]}{\partial \theta_i} u_s + u_r^T \frac{\partial [L_{rs}]}{\partial \theta_i} u_s + \frac{1}{2} u_r^T \frac{\partial [L_{rr}]}{\partial \theta_i} u_r \tag{3.1}$$

where $[L_{ss}]$ and $[L_{rr}]$ are the self-inductance matrixes of the stator and rotor respectively, and $[L_{sr}] = [L_{rs}]^T$ is the mutual inductance matrix; u_s is the stator current input vector and u_r is the polarity of the rotor. From this equation, the torque equation can be simplified based on the following assumptions: The core of the stator is non-ferromagnetic cores such as aluminum and plastic, which can cancel the first term. In addition, the rotor is composed of PMs, which can cancel the third term. Based on these assumptions, the torque equation can be approximated as a linear combination of stator currents:

$$T_{x,y,z} \approx u_r^T \frac{\partial [L_{rs}]}{\partial \theta_i} u_s = [K(q)] u_r^T u_s \tag{3.2}$$

where q is an orientation vector in spherical coordinate system; polar angle, azimuthal angle which mean the position angle and rotational angle which is related to driving directional rotation. From this equation, the current and torque can be represented as linear relation. The torque is generated by interactions between j^{th} stator pole pair and the kth rotor. Torque equation also can be represented as sum of magnetic torques between one PM and one EM. Then, the equation can be shown as following equation [7]:

$$T = \begin{bmatrix} T_x & T_y & T_z \end{bmatrix} = \sum_{j=1}^{n_s} T_{sj} = \sum_{j=1}^{n_s} \sum_{k=1}^{n_r} T_{jk} \tag{3.3}$$

where T_{sj} is a torque as a result of the interaction between j^{th} EM with n_r PMs, and T_{sj} is a torque as a result of the interaction between j^{th} EM with k^{th} PM.

The magnetic torque between j^{th} EM and the kth PM can be written in *xyz*-frame which is rotor frame.

$$T_{jk} = \begin{cases} 0 & if \ \left| s_j \times r_k \right| = 0 \\ u_{rk} u_{sj} f\left(\varphi_{j,k}\right) \dfrac{s_j \times r_k}{\left| s_j \times r_k \right|} & if \ \left| s_j \times r_k \right| > 0 \end{cases} \tag{3.4}$$

$$\varphi_{jk} = \left| \cos^{-1}\left(\frac{s_j^{\mathrm{T}} r_k}{\left| s_j \right| \left| r_k \right|} \right) \right| \tag{3.5}$$

where $\varphi_{j,k}$ is the separation angle between j^{th} stator pole pair and the kth rotor, and $f\left(\varphi_{jk}\right)$ is an approximate torque magnitude functions derived from the computed data using Data, u_{sj} is dimensionless current flowing through the jth EM, and u_{rk} is the polarity of the kth PM. From now on, **the torque equation 3.4** is simplified by using structural relation between EMs and PMs [12].

3.1 4 PM-1EM Model

From the design, SWM can be divided into repeating 10 sections, where each of them is composed of two columns of PM pairs. The two origin-symmetric EMs have equally directed and equally sized torque when the opposite currents are applied. This is because the arrangement of PMs is origin-symmetric and each PM on the opposite side have the opposite polarity. Therefore, the torque equation is only considerate for odd-numbered EMs which are located above XY-plane. Furthermore, the EMs in the first layer are always located on the xy-plane of the rotor frame because the range of the inclination is -16° to 16°. Based on this restriction, the shape of the section can be changed to the trapezoid which is made by neighboring 4PMs as shown in **Fig 3.2.1 (a).** This section can include one or no EM, because δ_s is bigger than δ_r and $2\beta_s$ is bigger than β_r. Furthermore, the relation between polarity of neighboring 4 PMs is opposite each other; $u_{sj} = -u_{sj+1} = -u_{sj+3} = u_{sj+4}$. Based on this relation, the torque equation of jth stator pole pair from four PMs which includes the jth EM can be represented as following:

$$T_{\Delta j} = u_{sj} \left(-1\right)^k \left[\begin{array}{c} f\left(\varphi_{j,k}\right) \dfrac{s_j \times r_k}{\left|s_j \times r_k\right|} - f\left(\varphi_{j,k+1}\right) \dfrac{s_j \times r_{k+1}}{\left|s_j \times r_{k+1}\right|} \\ -f\left(\varphi_{j,k+3}\right) \dfrac{s_j \times r_{k+3}}{\left|s_j \times r_{k+3}\right|} + f\left(\varphi_{j,k+4}\right) \dfrac{s_j \times r_{k+4}}{\left|s_j \times r_{k+4}\right|} \end{array} \right] \qquad (3.6)$$

where $T_{\Delta j}$ is a simplified torque term which is generated by j^{th} EM; k is an index:

$$\varphi_{j,k}, \varphi_{j,k+1}, \varphi_{j,k+3}, \varphi_{j,k+4} \leq \delta_r \qquad (3.7)$$

Simply, the section can be made with the four permanent magnets, and this section always includes one EM or not. Based on the section and the location of EM, the number of torque terms can be reduced from $n_s \times n_r$ to $2n_s \left(= 4m_s\right)$.

3.2 Coordinate transformation

In the **Section 3.1**, 4PM-1EM model is based on the rotor arrangement. Therefore, all equations about torque have to be induced only in the body frame, fixed at rotor. Now in **Section 3.2**, to simplify the cross-product term in the torque, local coordinate is introduced for each sections then the body frame is adapted. The adaptation follows Z-y'-z transformation which is shown below:

$$[\Gamma] = \begin{bmatrix} \cos\omega_3 & \sin\omega_3 & 0 \\ \sin\omega_3 & \cos\omega_3 & 0 \\ 0 & 0 & 1 \end{bmatrix} \begin{bmatrix} \cos\omega_2 & 0 & -\sin\omega_2 \\ 0 & 1 & 0 \\ \sin\omega_2 & 0 & \cos\omega_2 \end{bmatrix} \begin{bmatrix} \cos\omega_1 & \sin\omega_1 & 0 \\ -\sin\omega_1 & \cos\omega_1 & 0 \\ 0 & 0 & 1 \end{bmatrix} \quad (3.8)$$

where the values of $\omega_1, \omega_2, \omega_3$ are orientation angles in Z-y`-z coordinate frame.

The position vectors of stator poles in body frame satisfies following equation:

$$\hat{s}_j = [\Gamma] s_j = \begin{bmatrix} \hat{s}_{j1} & \hat{s}_{j2} & \hat{s}_{j3} \end{bmatrix} \quad (3.9)$$

From the position vector of stator poles in body frame, the new angles ϕ and θ are defined in **Fig. 3.2.1**; ϕ_j is the angle between the projection of s_j on $x_i y_i$-plane from the x_i-axis and θ_j is the angle between s_j and $x_i y_i$-plane;

$$\phi_j = \tan^{-1}\left(\frac{\hat{s}_{j2}}{\hat{s}_{j1}}\right) - \left[\frac{\tan^{-1}\left(\frac{\hat{s}_{j2}}{\hat{s}_{j1}}\right)}{\delta_r}\right] \quad (3.10)$$

$$\theta_j = \sin^{-1}\left(\hat{s}_{j3}\right)$$

where (x_i, y_i, z_i) is the newly defined coordinate systems based on the divided sections.

There are two new coordinate systems, (x_i, y_i, z_i), and (x_j, y_j, z_j). (x_i, y_i, z_i) is the section coordinate system as mentioned above, which requires the coordinate relation between EM and 4PMs. (x_j, y_j, z_j) is defined on the jth EM as shown in **Fig 3.2.1 (b)** to simplify the cross product equation; x_j direction is same with the center-to-EMs coordinate, and y_j direction is parallel to xy-plane.
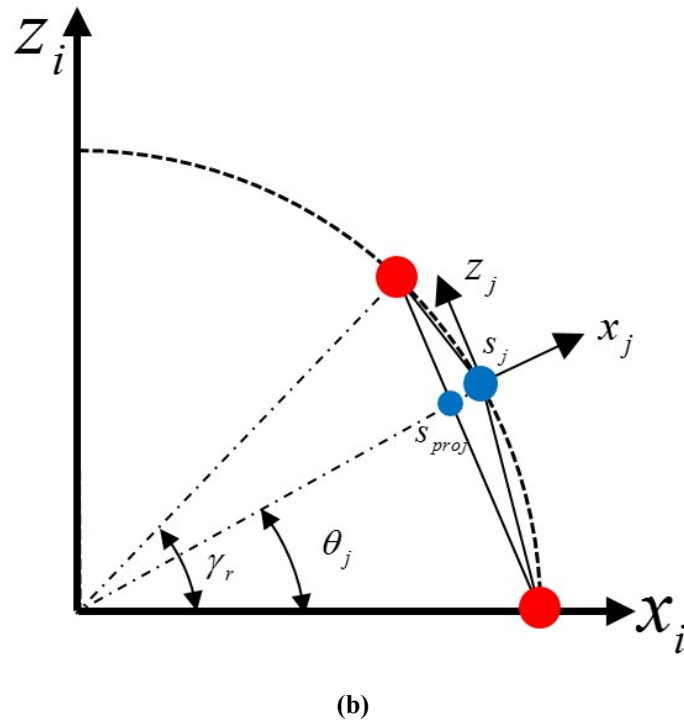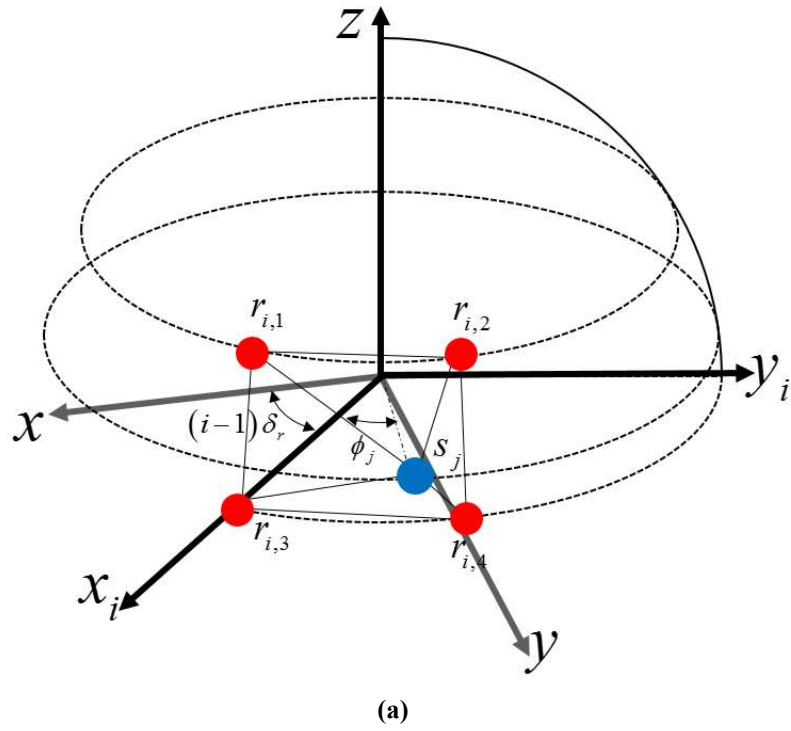
(a)

(b)

Fig. 3.2.1 The coordinate systems $\left(x_i, y_i, z_i \right)$ **and** $\left(x_j, y_j, z_j \right)$ **and new defined angle**

(x_i, y_i, z_i) is represented as following equation:

$$\begin{bmatrix} x_i \\ y_i \\ z_i \end{bmatrix} = \begin{bmatrix} C_{(i-1)\delta_r} & S_{(i-1)\delta_r} & 0 \\ -S_{(i-1)\delta_r} & C_{(i-1)\delta_r} & 0 \\ 0 & 0 & 1 \end{bmatrix} \begin{bmatrix} x \\ y \\ z \end{bmatrix} = [\Gamma_i] \begin{bmatrix} x \\ y \\ z \end{bmatrix} \tag{3.11}$$

where i is the section number which has the range of 1 to 10. The $[\Gamma_i]$ is the coordinate transformation matrix body to new coordinate frame; $C_{(i-1)\delta_r} = \cos(i-1)\delta_r$; $S_{(i-1)\delta_r} = \sin(i-1)\delta_r$. The relation between (x_i, y_i, z_i) and (x_j, y_j, z_j) is shown below:

$$\begin{bmatrix} x_j \\ y_j \\ z_j \end{bmatrix} = \begin{bmatrix} -C_{\phi_j} C_{\theta_j} & -S_{\phi_j} C_{\theta_j} & S_{\theta_j} \\ -S_{\phi_j} & C_{\phi_j} & 0 \\ -C_{\phi_j} S_{\theta_j} & -S_{\phi_j} S_{\theta_j} & C_{\theta_j} \end{bmatrix} \begin{bmatrix} x_i \\ y_i \\ z_i \end{bmatrix} = [\Gamma_{ij}] \begin{bmatrix} x_i \\ y_i \\ z_i \end{bmatrix} \tag{3.12}$$

where $[\Gamma_{ij}]$ is the coordinate transformation matrix coordinate system of (x_i, y_i, z_i) to coordinate system of (x_j, y_j, z_j); the $C_{\phi_i} = \cos \phi_i$; $S_{\phi_i} = \sin \phi_i$; $C_{\theta_i} = \cos \theta_i$; $S_{\theta_i} = \sin \theta_i$. An important thing in this equation is the definition of angle ϕ_j which means that the jth EM is in the ith section.

From these newly defined angles and positions, the separation angle between stator and rotor can be derived using dot product relation as shown below:

$$\begin{aligned} \varphi_{j,1} &= \arccos\big(\cos(\beta_r)\cos(\theta_j)\cos(\phi_i) + \sin(\beta_r)\sin(\theta_j)\big) \\ \varphi_{j,2} &= \arccos\big(\cos(\beta_r)\cos(\theta_j)\cos(\delta_r - \phi_i) + \sin(\beta_r)\sin(\theta_j)\big) \\ \varphi_{j,3} &= \arccos\big(\cos(\theta_j)\cos(\phi_i)\big) \\ \varphi_{j,4} &= \arccos\big(\cos(\theta_j)\cos(\delta_r - \phi_i)\big) \end{aligned} \tag{3.13}$$

where $\varphi_{j,1}$ is the separation angles from j^{th}. The numbering is shown in **Fig. 3.3.1**. These separation angles are used to calculate the magnitude of torque using toque function. After the explanation of the simplified cross-product term in the **Section 3.3**, the torque function is explained in the **Section 3.4**.

3.3 Cross-product term

In this section, the unit cross-product term $\left(\dfrac{s_j \times r_k}{|s_j \times r_k|}\right)$ is simplified based on the definition of the cross-product. From the definition, the cross product is defined by the formula; $a \times b = n \|a\|\|b\|\sin\theta$.

n is a unit vector perpendicular to the plane contacting a and b. Briefly, only the perpendicular terms are considered when unit cross product is simplified. **Figure 3.3.1 (a)** shows the example of torque which is caused by one PM and one EM. In that case, x_j-direction is ignored. So the x_j-directional force can be ignored in the (x_j, y_j, z_j) coordinate system. Based on this, the unit cross product vector can be represented by two components y_j, z_j. The direction of torques is shown in **Fig 3.3.1 (b)**. The equation of unit cross product is replaced by following equation:

$$\frac{s_j \times r_k}{|s_j \times r_k|} = \frac{-h_{jk}y_j - l_{jk}z_j}{\sqrt{h_{jk}^2 + l_{jk}^2}} = -C_{jk}y_j - S_{jk}z_j \tag{3.14}$$

The values of h_i $(i = 1, 2)$ and l_i $(i = 1, 2, 3, 4)$ can be calculated by using trapezoid structure and location of jth EM. l_i can be calculated by trigonometric functions. Each values are represented as following equations:

$$l = l_2 + l_4 = 2R\sin\left(\frac{\delta_r}{2}\right)$$
$$l_1 = \frac{\sin(\phi)}{\sin(108° - \phi)\cos(\gamma_r)}$$
$$l_2 = \frac{\sin(\phi)}{\sin(108° - \phi)} \tag{3.15}$$
$$l_3 = l\cos(\gamma_r) - l_1$$
$$l_4 = l - l_2$$

where l_1 is the length between the rotor $r_{i,1}$ and the projection point of s_j on the chord $r_{i,1}r_{i,2}$. l_2, l_3, l_4 are calculated similarly. The values are shown in **Fig. 3.3.1**

(a)   (b)
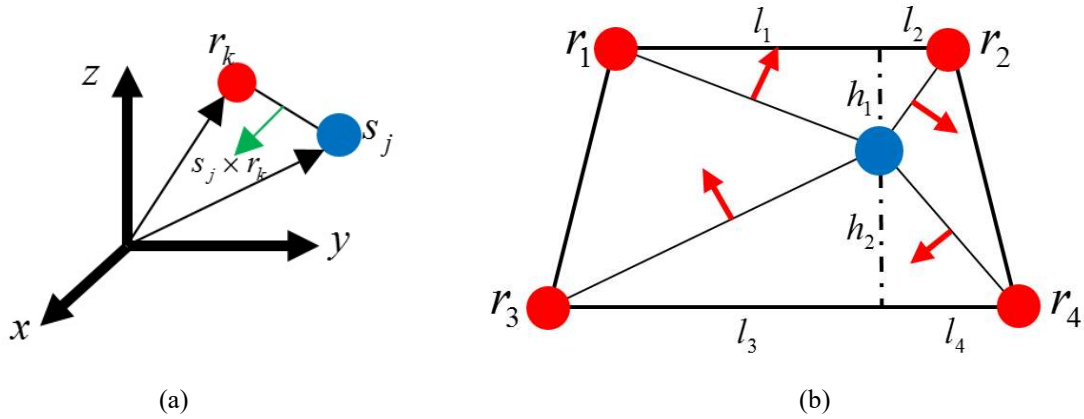
Fig 3.3.1 The cross product directions (a) example of relation between EM and PM (b) the notations for calculating unit cress products and directions of cross products

With these values, h_i can be calculated by following order. The location of the stator in the body frame can be represented as:

$$s_j = \begin{bmatrix} \cos\theta_{jk}\cos\phi_{jk} & \cos\theta_{jk}\sin\phi_{jk} & \sin\theta_{jk} \end{bmatrix} \tag{3.16}$$

The location of stator at the trapezoid plane which includes 4 PMs can be represented as:

$$s_{planar} = ts = \begin{bmatrix} t\cos\theta_{jk}\cos\phi_{jk} & t\cos\theta_{jk}\sin\phi_{jk} & t\sin\theta_{jk} \end{bmatrix} \tag{3.17}$$

s_{planar} is an intersection of line $s_j o$ and the plane include trapezoid. Therefore, the s_{planar} exists on the plane which includes trapezoid section. The ratio of $s_j o$ and $s_{planar} O$ is shown below:

$$t = \frac{\sin\delta_r \sin\gamma_r}{\sin\delta_r \sin\gamma_r \cos\theta\cos\phi + \sin\gamma_r \cos\theta\sin\phi(1-\cos\delta_r) + \sin\delta_r \sin\theta(1-\cos\gamma_r)} \tag{3.18}$$

Then, the value of h_i can be calculated by using formula of the distance between the location of s_{planar} and the line $r_{i,1}r_{i,2}$ in three-dimensional space. It can be represented as following equation:

$$h_1 = \frac{\sqrt{\begin{array}{l}\left(\cos\gamma_r\sin\delta_r\left(t\sin\theta-\sin\gamma_r\right)\right)^2+\left(\cos\gamma_r\left(1-\cos\delta_r\right)\left(t\sin\theta-\sin\gamma_r\right)\right)^2\\+\cos\gamma_r\left(\cos\theta\sin\phi\left(\cos\delta_r-1\right)-\sin\delta_r\left(t\cos\theta\cos\phi-\cos\gamma_r\right)\right)\end{array}}}{\cos\gamma_r\sqrt{2-2\cos\delta_r}}$$

(3.19)

$$h_2 = \frac{\sqrt{\begin{array}{l}\left(t\sin\delta_r\sin\theta\right)^2+\left(t\left(1-\cos\delta_r\right)\sin\theta\right)^2\\+\left(\left(t\cos\theta\cos\phi-1\right)\sin\delta_r+t\left(1-\cos\delta_r\right)\cos\theta\sin\phi\right)^2\end{array}}}{\sqrt{2-2\cos\delta_r}}$$

l_i and h_i are calculated by the function of ϕ and θ. With these values, the unit cross product

satisfies $\dfrac{s_j\times r_{i,1}}{\left|s_j\times r_{i,1}\right|}\approx s_{j1}$ and $s_{j1}\bullet\left(l_1 y_k-h_1 z_k\right)=0$. Therefore, the approximate unit cross product

can be represented as:

$$s_{j1}=\begin{bmatrix}0\\-C_{j1}\\-S_{j1}\end{bmatrix}^T\begin{bmatrix}x_j\\y_j\\z_j\end{bmatrix}$$

(3.20)

Similarly,

$$s_{j2}=\begin{bmatrix}0\\-C_{j2}\\S_{j2}\end{bmatrix}^T\begin{bmatrix}x_j\\y_j\\z_j\end{bmatrix},s_{j3}=\begin{bmatrix}0\\C_{j3}\\-S_{j3}\end{bmatrix}^T\begin{bmatrix}x_j\\y_j\\z_j\end{bmatrix},s_{j4}=\begin{bmatrix}0\\C_{j4}\\S_{j4}\end{bmatrix}^T\begin{bmatrix}x_j\\y_j\\z_j\end{bmatrix}$$

(3.21)

where $C_{j1}=h_1/\sqrt{h_1^2+l_1^2};S_{j1}=l_1/\sqrt{h_1^2+l_1^2}$, $C_{j2}=h_1/\sqrt{h_1^2+l_2^2};S_{j2}=l_2/\sqrt{h_1^2+l_2^2}$,

$C_{j3}=h_2/\sqrt{h_2^2+l_3^2};S_{j3}=l_3/\sqrt{h_2^2+l_3^2}$, $C_{j4}=h_2/\sqrt{h_2^2+l_4^2};S_{j4}=l_4/\sqrt{h_2^2+l_4^2}$.

Based on these values and coordinate transformation, the unit cross product can be represented as:

$$s_{j1}=\begin{bmatrix}0\\-C_{j1}\\-S_{j1}\end{bmatrix}^T\begin{bmatrix}x_j\\y_j\\z_j\end{bmatrix}=\left[\Gamma_i\right]^T\left[\Gamma_{ij}\right]^T\begin{bmatrix}0\\-C_{j1}\\-S_{j1}\end{bmatrix}^T\begin{bmatrix}x\\y\\z\end{bmatrix}$$

(3.22)

In the **Section 3.4**, the torque model is simplified by using simplified unit cross-product term.

3.4 Simplified Torque Model

Previously, the torque model of 4PM-1EM model is given by:

$$
T_{\Delta j} = u_{sj}\left(-1\right)^{i}
\begin{bmatrix}
f\left(\varphi_{j,k}\right)\dfrac{s_j \times r_k}{\left|s_j \times r_k\right|} - f\left(\varphi_{j,k+1}\right)\dfrac{s_j \times r_{k+1}}{\left|s_j \times r_{k+1}\right|} \\[2mm]
-f\left(\varphi_{j,k+3}\right)\dfrac{s_j \times r_{k+3}}{\left|s_j \times r_{k+3}\right|} + f\left(\varphi_{j,k+4}\right)\dfrac{s_j \times r_{k+4}}{\left|s_j \times r_{k+4}\right|}
\end{bmatrix}
\qquad (3.23)
$$

The simplified torque mode can be applied to 4EM-1PM model, then the torque $T_{\Delta j}$ can be replaced as following form:

$$
T_{\Delta i} = u_{sj}\left(-1\right)^{i}
\left(
\begin{aligned}
&\begin{pmatrix} -f\left(\varphi_{j,k}\right)C_{\mu_{j,k}} - f\left(\varphi_{j,k+1}\right)C_{\mu_{j,k+1}} \\ +f\left(\varphi_{j,k+3}\right)C_{\mu_{j,k+3}} + f\left(\varphi_{j,k+4}\right)C_{\mu_{j,k+4}} \end{pmatrix}
\begin{bmatrix} -S_{(2i-1)\delta_r/2} \\ C_{(2i-1)\delta_r/2} \\ 0 \end{bmatrix}^{\mathrm{T}}
\begin{bmatrix} \hat{x} \\ \hat{y} \\ \hat{z} \end{bmatrix} \\[2mm]
+&\begin{pmatrix} -f\left(\varphi_{j,k}\right)S_{\mu_{j,k}} + f\left(\varphi_{j,k+1}\right)S_{\mu_{j,k+1}} \\ -f\left(\varphi_{j,k+3}\right)S_{\mu_{j,k+3}} + f\left(\varphi_{j,k+4}\right)S_{\mu_{j,k+4}} \end{pmatrix}
\begin{bmatrix} -S_{\theta_{j,k+1}}C_{(2i-1)\delta_r/2} \\ -S_{\theta_{j,k+1}}S_{(2i-1)\delta_r/2} \\ C_{\theta_{j,k+1}/2} \end{bmatrix}^{\mathrm{T}}
\begin{bmatrix} \hat{x} \\ \hat{y} \\ \hat{z} \end{bmatrix}
\end{aligned}
\right)
\qquad (3.24)
$$

where the subscript i is the section number from 1 to 10. With **Equation 3.3 and 3.24**, torque-current relation can be simplified as:

$$
T = 2\sum_{i=1}^{10} T_{\Delta i} = KU
\qquad (3.25)
$$

The matrix T is the total torque matrix (3 x 1 matrix). Matrix K is the torque matrix of torque-current relation (3 x 8 matrix). Matrix U is the current matrix which means currents of coils (8 x 1 matrix). The torque can be calculated by closed- form.

3.5 Torque function

The torque function is calculated based on the simulation data; the conditions of simulation are same as the actual SWM models (1EM and 1PM) with 1A of current in coil. The two methods are used for the simulation. The one is finite-element (FE) method and other is Distributed Multi-pole (DMP) method. The COMSOL is the program which is one of popular programs for analysis magnetic fields based on FE method. The DMP method is used by many researchers to analyze actuator design involving permanent magnets because of compact formulation/solutions and intuitive magnetic fields.

The DMP is based on the concept that one magnet consists of a number of magnetic dipole moments. Then the magnetic field can be expressed as a combination of finite number of dipole moments. The method is originally used to analyze PMs [13]. Then, it is subsequently expanded to EMs generating time-varying magnetic field [14], [15]. **Fig 3.5.1 (a) and (b)** show that the dipoles are distributed on two layers inside a cylindrical PM and EM. A dipole moment can be obtained in **Fig. 3.5.1 (c)**.

(a) PM modeling (b) EM modeling (c) A dipole moment
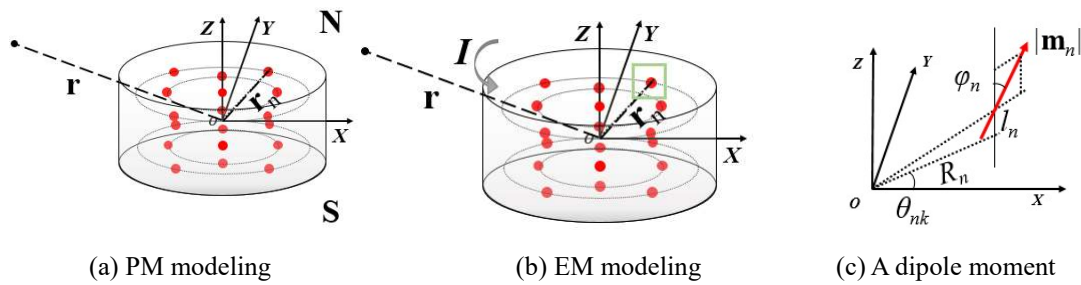
Fig.3.5.1 extended Distributed Multi-Pole (eDMP) geometry of cylindrical coil

The dipole moments should be arranged to characterize the magnetic field of the coil using modelling parameters; the position $\mathbf{r}_{nk}$ and the dipole moment are expressed in **Equation 3.26 and 3.27**.

$$\mathbf{r}_{nk} = [R_n \cos\theta_{nk} \quad R_n \sin\theta_{nk} \quad \pm l_n]^{\mathrm{T}} \tag{3.26}$$

$$\mathbf{m}_{nk} = |\mathbf{m}_n| [\cos\theta_{nk} \sin\phi_n \quad \sin\theta_{nk} \sin\phi_n \quad \cos\phi_n]^{\mathrm{T}} \tag{3.27}$$

where R_n and l_n are the radius and height of the nth layer, respectively. Additionally, ϕ_n and $|\mathbf{m}_n|$ are the orientation and strength of a dipole moment on the layer, respectively. $\theta_{nk} = 2\pi(k-1)/N_k$; $k = 1, 2, ..., N_k$ and $n = 1, 2, ..., N_n$ where N_k is the number of dipoles

on a specific layer, and N_n is the number of layers.

Based on the dipoles, the magnetic flux density (MFD) **B,** and the magnetic vector potential (MVP) **A** at an arbitrarily position **r,** are obtained by **Equation 3.28 and 3.29** as the summation of all the dipoles.

$$\mathbf{B}(\mathbf{r}) = \frac{\mu_0}{4\pi} \sum_{n=1}^{N_n} \sum_{k=1}^{N_k} \frac{3\left(\mathbf{m}_{nk} \bullet \left(\mathbf{r} - \mathbf{r}_{nk}\right)\right)\left(\mathbf{r} - \mathbf{r}_{nk}\right)}{\left|\mathbf{r} - \mathbf{r}_{nk}\right|^5} - \frac{\mathbf{m}_{nk}}{\left|\mathbf{r} - \mathbf{r}_{nk}\right|^3}$$

(3.28)

$$\mathbf{A}(\mathbf{r}) = \frac{\mu_0}{4\pi} \sum_{n=1}^{N_n} \sum_{k=1}^{N_k} \frac{\mathbf{m}_{nk} \times \left(\mathbf{r} - \mathbf{r}_{nk}\right)}{\left|\mathbf{r} - \mathbf{r}_{nk}\right|^3}$$

(3.29)

where μ_0 is the permeability of free space.

The design parameters can be computed by minimizing the error between the predetermined magnetic field and the field as written in **Equation 3.28 and 3.29**. The parameters for the magnetic dipoles, N_k and N_n, are initially set but increase when the error of field is not acceptable. Analytical or numerical methods could be used as a reference for the MFD in **Equation 3.30**, and for the MVP in **Equation 3.31 and 3.32** to compute the dipole moments.

$$Error = \sum_{j=1}^{N_j} \left|\mathbf{B}_j^{Ref} - \mathbf{B}_j^{eDMP}\right|^2 \leq E_{DMP}$$

(3.30)

$$\mathbf{V}\begin{bmatrix} \mathbf{m}_{11} \\ \vdots \\ \mathbf{m}_{N_n N_k} \end{bmatrix} = \begin{bmatrix} A_1 \\ \vdots \\ A_{N_i} \end{bmatrix}$$

(3.31)

$$\mathbf{V}_{i,nk} = \frac{\mu_0}{4\pi d^3} \begin{bmatrix} 0 & z & -y \\ -z & 0 & x \\ y & -x & 0 \end{bmatrix}$$

(3.32)

where E_{DMP} is the maximum allowable error. Correspondingly, $\mathbf{r}_d = \mathbf{r}_i - \mathbf{r}_{rk}$ and $d = \left|\mathbf{r}_d\right|$ $\left(i = 1, 2, .., N_i, j = 1, 2, .., N_j\right)$ where N_i and N_j are the number of positions where the MFD and the MVP are maximum.

Lorentz force $\mathbf{F}$ and torque at the origin, $\mathbf{T}_O$ can be computed from PM and EM dipole moments interaction, the torque from two kinds of stator coil are compared. They are described in **Equation 3.33 and 3.34**

$$\mathbf{F}(\mathbf{r}_j) = \frac{3\mu_0}{4\pi} \sum_{i=1}^{N_{EM}} \frac{1}{|\mathbf{r}_{ji}|^5} \begin{bmatrix} (\mathbf{m}_j \bullet \mathbf{r}_{ji})\mathbf{m}_i + (\mathbf{m}_i \bullet \mathbf{r}_{ji})\mathbf{m}_j \\ +(\mathbf{m}_i \bullet \mathbf{m}_j)\mathbf{r}_{ji} \\ -5(\mathbf{m}_i \bullet \widehat{\mathbf{r}_{ji}})(\mathbf{m}_i \bullet \widehat{\mathbf{r}_{ji}})\mathbf{r}_{ji} \end{bmatrix}$$

(3.33)

$$\mathbf{T}_O = -\sum_{j=1}^{N_{PM}} \left[\mathbf{m}_j(\mathbf{r}_j) \times \left(\sum_{i=1}^{N_{EM}} \mathbf{B}_i(\mathbf{r}_j) \right) \right] + \left[\mathbf{r}_j \times \mathbf{F}(\mathbf{r}_j) \right]$$

(3.34)

where $\mathbf{m}_j$ is a jth dipole moment of PMs ($j=1,2,...,N_{PM}$); $\mathbf{m}_i$ is a ith dipole moment of EMs ($i=1,2,...,N_{EM}$); $\mathbf{r}_j$ is a position of $\mathbf{m}_j$, $\mathbf{r}_i$ is a position of $\mathbf{m}_i$; $\mathbf{r}_{ji}=\mathbf{r}_j-\mathbf{r}_i$.

During this part, the torque function is calculated with two cases: using only one PM on inner rotor and using PM pairs on inner and outer rotor. The first case aims to check the state of EMs such as temperature and gap caused by magnetic force and vibration etc. The resulting data of first case is in **Fig 3.5.2**. The COMSOL data has some fluctuation caused by numerical errors as shown in **Fig 3.5.2 (a)**. Contrastively, DMP data has no fluctuation as shown in **Fig 3.5.2 (b)**. The curve-fitting is applied to calculate torque at any angles.
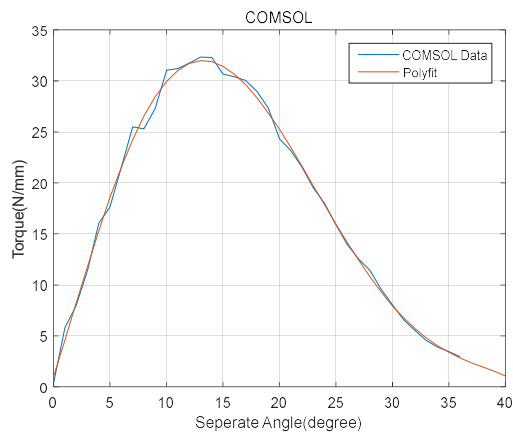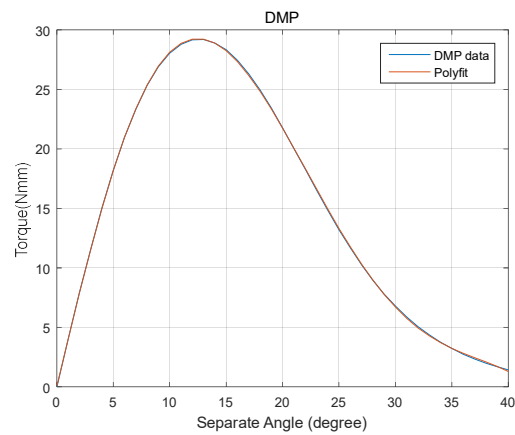
(a) Data and Function of COMSOL   (b) Data and Function of DMP

Fig.3.5.2 The Simulation Data and Torque function using only inner PM

$$p_{COMSOL} = 10^4 \left[0.2509 \ -0.9054 \ 1.0920 \ -0.5082 \ 0.0430 \ 0.0195 \ 0.0001 \right]$$

$$p_{DMP} = 10^4 [0.2940 \ -0.9369 \ 1.0199 \ -0.4146 \ 0.0094 \ 0.0225 \ 0.0000]$$

p_{DMP} and p_{COMSOL} are the result using the MATLAB function 'polyfit; sixth order' with the data of COMSOL and DMP. The function relation is between angle(rad) to torque. In case of COMSOL curve fitting function, the torque value is 1.0581Nmm when input separate angle is zero. The value of torque should be zero when separate angle is zero because of the characteristics of magnetic fields and structural restriction. While in case of DMP curve fitting function, the value of torque is zero when separate angle is zero.

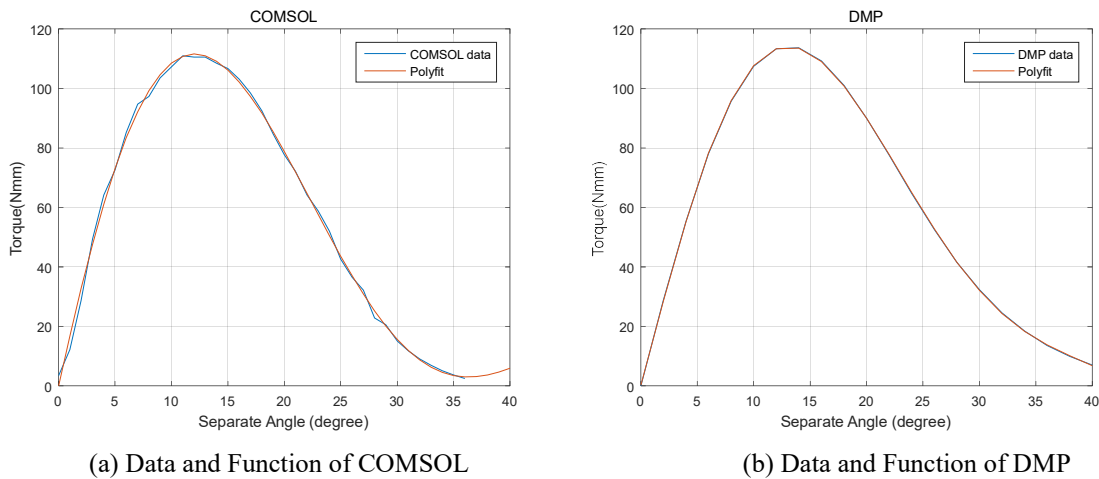The second case that PM pairs are used with EM is shown below:

(a) Data and Function of COMSOL   (b) Data and Function of DMP

Fig.3.5.3 The Simulation Data and Torque function using inner and outer PMs

$$p_{COMSOL} = 10^4 \left[0.5520 \ -2.0741 \ 2.4458 \ -0.9168 \ -0.1193 \ 0.0999 \ -0.0000 \right]$$

$$p_{DMP} = 10^4 [1.1869 \ -3.6720 \ 4.0056 \ -1.7005 \ 0.0897 \ 0.0796 \ 0.0000]$$

In the case of COMSOL curve fitting function, the torque value is -0.3123Nmm when input separate angle is zero. The value of torque also should be zero when separate angle is zero. In case of DMP curve fitting function, the value of torque is zero when separate angle is zero. Comparing the first cases, the COMSOL data has less fluctuation. The torque function based on DMP methods is used for the control system after the position control experiment.

3.6 Comparison of COMSOL, DMP, Experiment and Simplified Model

The comparison is required to make sure the propriety of simplified equation before position control. Previously, there are experimental results in shape of coil section. With the same simulation set-up, the comparison of Experiment, COMSOL, DMP, and Simplified torque model is done:

(a)   (b)
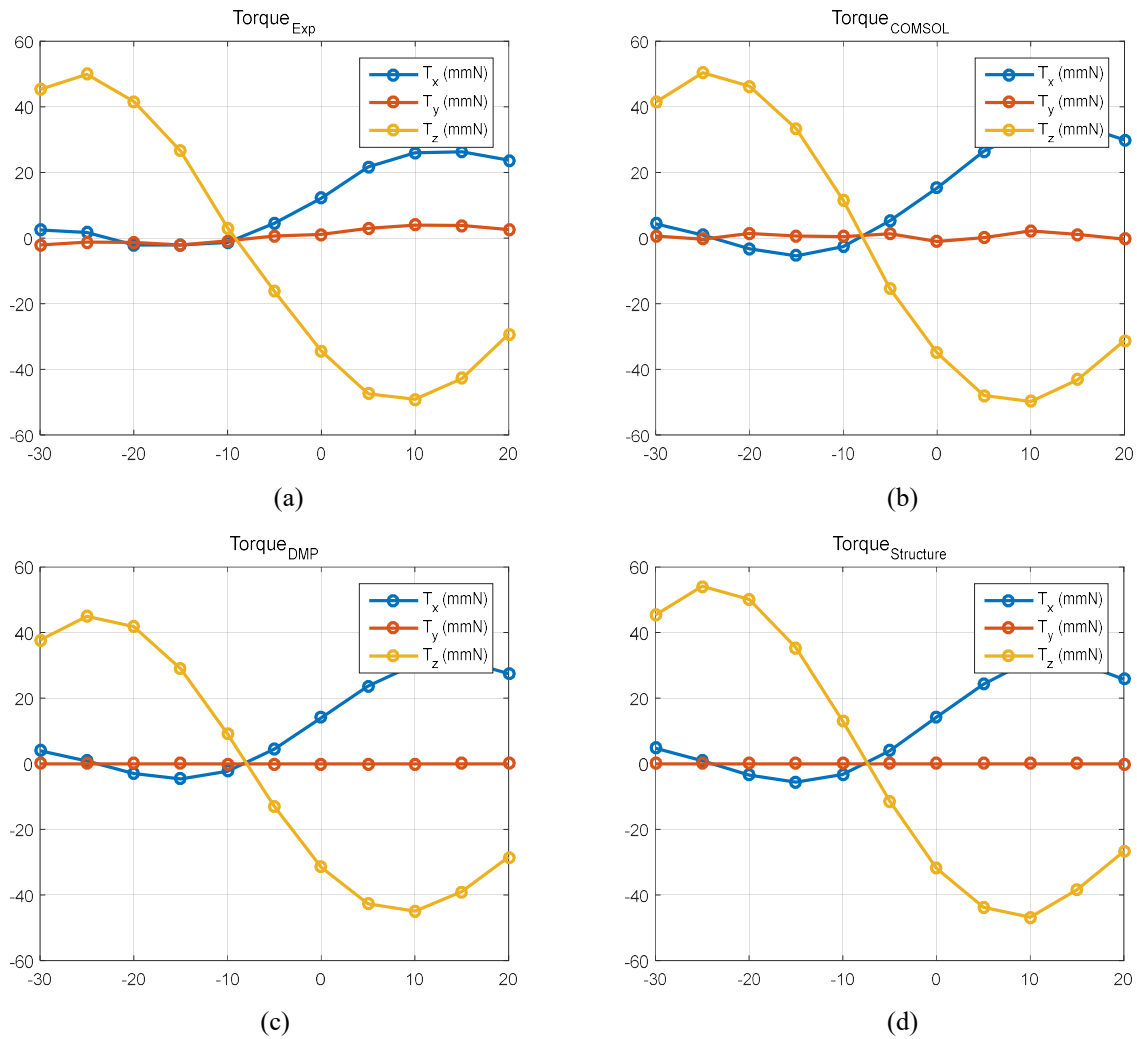
(c)   (d)

Fig 3.6.1 The torque graphs; 6 PM and 1 EM cases (a) Experiment results (b) COMSOL simulation results (c) DMP simulation results (d) Simplified equation model simulation results

All results show the similar trends. For an accurate comparison, the comparison graph on each directional torque and error are drawn:
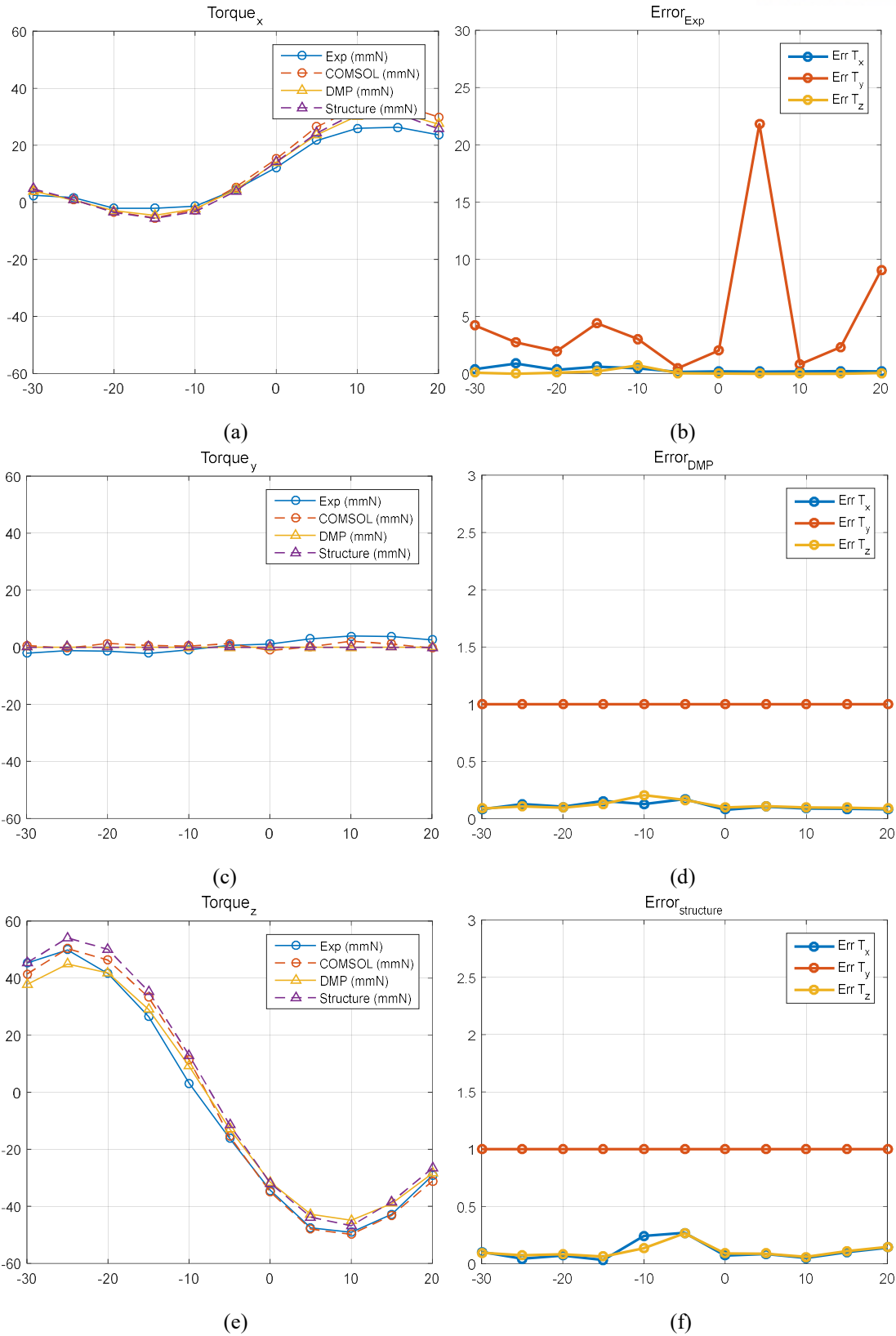
(a)

(b)

(c)

(d)

(e)

(f)

Fig. 3.6.2 The graphs for comparison (a) T_x **graphs (b) the error about experiment and COMSOL results (c)** T_y **graphs (d) the error about DMP and COMSOL results (e)** T_z **graphs (f) the error about Simplified model and COMSOL results**

As shown in **Fig. 3.6.2**, the comparison graphs, the experiment data showed a little bit smaller torque magnitude than the simulation results. On the other hands, the error graphs showed various trends. In those graphs, the y-axes represented the relative error; COMSOL simulation showed the true value, and the others showed the approximation. The error is calculated by following equation:

$$error = \left| \frac{x - x_{comsol}}{x_{comsol}} \right|$$
(3.35)

where the x is the comparison value such as experiment, DMP, and Simplified model data; and x_{COMSOL} is the experiment value. (Because the COMSOL is a generally used program for simulations, the COMSOL value is chosen as the true value.) The **Figure 3.6.2 (b)** shows that the relative error of T_y is roughly 22 where the COMSOL value of T_y is almost zero. (Theoretically, the T_y value become zero when EM locate at the middle of two PM columns.) On the other hands, the relative error of T_y is 1 in **Figure 3.6.2 (d) and (f)**. In other words, the simulation results of DMP and the simplified model have zero values for T_y. It correspond with the theoretical prediction results. The relative errors of T_x and T_z in the experiments are less than 1. Those in DMP are less than 0.3 and those in simplified model are less than 0.4.

Furthermore, the computation time is checked during the simulation of COMSO, DMP and Simplified Model. Because, the purpose of the simplified model is the real-time control by reducing computation time. The computation time mean only the calculation time excluding the plotting time. For each models, the computational times are: 118 sec for COMSOL, 5.8 sec for DMP, and 0.03 sec for the simplified equation. The results show that the computational times are dramatically reduced from COMSOL to the simplified equation model.

IV. Position Control

The final purpose of this study is the position control using the simplified torque equations. In this section, the principle and mechanism of position control will be introduced.

4.1 Holding torque

The state of rotor orientation is controlled by the principle of push-pull operation. When a stuff is held by two fingers, the two fingers apply certain pressure to the stuff. Similarly, the rotor is held by magnetic force generated by the stator. In the magnetic force, attractive and repulsive forces occur.
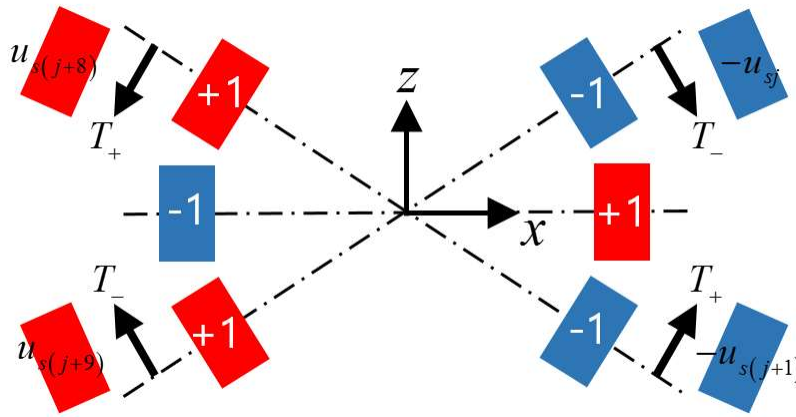

Fig. 4.1.1 Two EM layers and Three PM layers Holding torque

Fig. 4.1.1 shows the applied torque when the arrangement of PMs and EMs are same with SWM design which has three PM layers and two EM layers. In this case, $u_{s(j+1)}$ and $u_{s(j+8)}$ generate positive torque T_+ along with y-axis. $u_{s(j+1)}$ and $u_{s(j+8)}$ generate negative torque T_-. The torque model is written as the following form using push-pull operation:

$$T = T_+ + T_- + \Delta T \qquad (4.1)$$

where $T_\pm$ are the static torques and ΔT is the dynamic torque. The static torque is used to hold rotor to the desired position states and the dynamic torque is used to move motors. During this work, the external torque and the driving torque are not required for the position control. Therefore, the positive holding torque and the negative holding torque have the same magnitude with different sign each other. Then, the steady state of the maintaining position state requires zero for the total torque. However, the

current of coils are zero when total torque is zero. So, two groups are made to generate positive and negative torque, respectively. The "group 1" is composed of 1st, 3rd, 5th, and 7th coils and the "group 2" is composed of 9th, 11th, 13th, and 15th coils as shown **Fig. 4.1.2**.
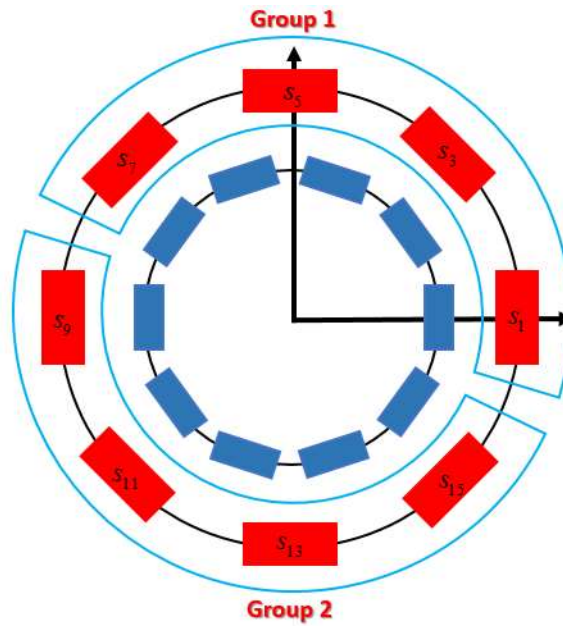

Fig. 4.1.2 The group of coils of stator to make positive and negative holding torque

Based on these groups, the torque matrix is also represented by two equations:

$$T_+ = K_+ U_1$$
$$T_- = K_- U_2$$

(4.2)

where K_+ is the positive torque matrix which is composed of first four columns of matrix K; K_- is the negative torque matrix which is composed of remaining four columns of matrix K; U_1 and U_2 are the current matrix for the group 1 and group 2, respectively.

4.2 Control Mechanism

During this work, there are no sensing system. The control system for the experiment is the open-loop control. Also the goal of this work is the position control, in the steady state. The experiment is started at the home-position then changed to the desired position. Therefore, when the desired angle is entered to the control mechanism, the current changed discontinuously. **Fig. 4.2.1** is a brief diagram of the control mechanism:
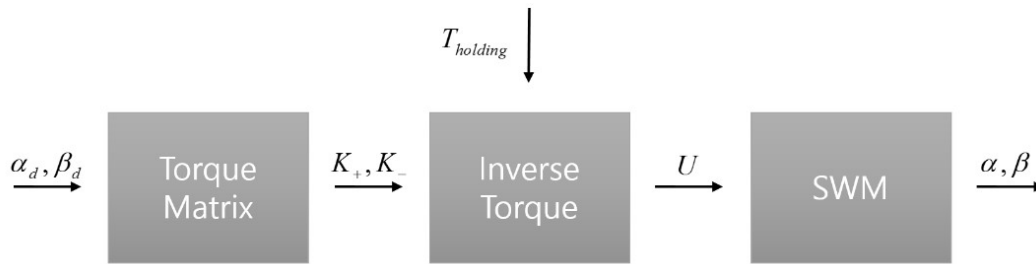

Fig. 4.2.1 The Control mechanism Diagram

where α_d, β_d, and $T_{holding}$ are input values. α_d and β_d are the desired angles, in other words the position input. $T_{holding}$ is the decided holding torque magnitude. $T_{holding}$ has the following relation:

$$T_+ = T_{holding}$$
$$T_- = -T_{holding}$$

(4.3)

The holding torque can make various types of vectors. In this paper, one of the most suitable holding torque vector is selected. The holding torque vector for this experiment is a vector designed to indicate the *y*-axis rotation.

The process of control system is as following. First, the desired position angle is entered into the control system. Then torque matrix is obtained from the simplified model. Using this torque matrix with holding torque input, the currents are calculated by using pseudo-inverse, because the torque matrix is 3×1 matrix, the two torque matrix is 3×4 matrix and the current matrix is 4×1 matrix. After the calculation, the currents are applied to actual SWM.
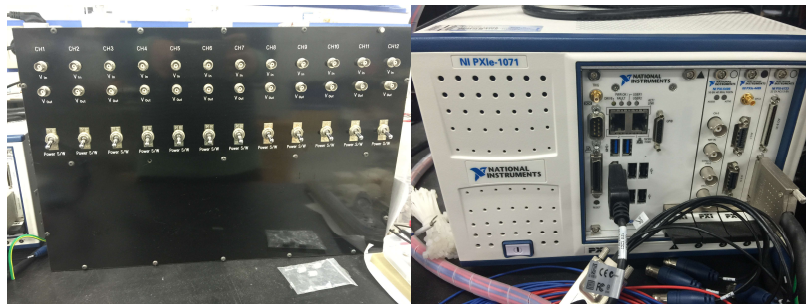
V. Experiment

5.1 Experimental set-up

There are two types of set-ups; Hardware and Software set-ups. For the Hardware set-up, the SWM and control set-up are required. As mentioned above, the control set-up is required to currents control of each coil cases. For the experiment, the current is applied by the servo-amplifier (*Junus*, made by copely control Co.), shown in **Fig 5.1.1 (a)** - *Junus* is developed to control the conventional motor systems. The specifications of the *Junus* is that the maximum output voltage is 90V, continuous maximum ampere is 10A and peak ampere is 20A – To protect coils from overheated, the scaling setting of Junus is 2A when the input voltage is 10V. The relation between the input and output is linear. Also, the maximum continuous ampere is set to 1.8A and the peak ampere is set to 2A. But the *Junus* have one serial port. So a control box is prepared, which could connect 12 *Junus* including four spares. It is shown in **Fig. 5.1.1 (b)**. The *Junus* can be connected by two sockets in the front. They offer the input and output voltages. At the back of the control box, there are each RS-232 communication socket of *Junus* and two 24 parallel ports which are connected to all of input and output voltage sockets of *Junus*, respectively. The multiple analog output voltage device is required to apply the voltage to these *Junus*s. It is *NI 6723*, shown in **Fig 5.1.1 (c)**; this is a National Instruments product which can offer 32 output voltages and the range is ± 10 V. The voltage signals of the *NI 6723* is applied to *Junus*s through the DAQ.

(a) Servo-amplifier; Junus

(b) Control Box   (c) NI-6723; multiple analogue output device

Fig. 5.1.1 The currents control experimental set-up

The SWM set-up is based on the motor design part (**Chap II**). The set-up is shown in **Fig 5.1.2.** During this experiment, the outer rotors are not set and only EMs of stator are used for the easier approach to the EMs. The coils are manufactured as: the starting wire and the finishing wire are located at the same face of the coil, the thickness is 26 AWG, the small coil is winded counter-clockwise and large coil is winded clockwise to be connected. Because there is no sensing system, the position of SWM is analyzed with the visual information. The motor structure is symmetric, therefore, there are marks at rotor and stator for the position sensing. The angle gauge is attached to the upper stator ring and the cross mark which indicated x and y axes is attached to the upper side of rotor. With this gauge and shaft attached at rotor, the position of rotor is measured.
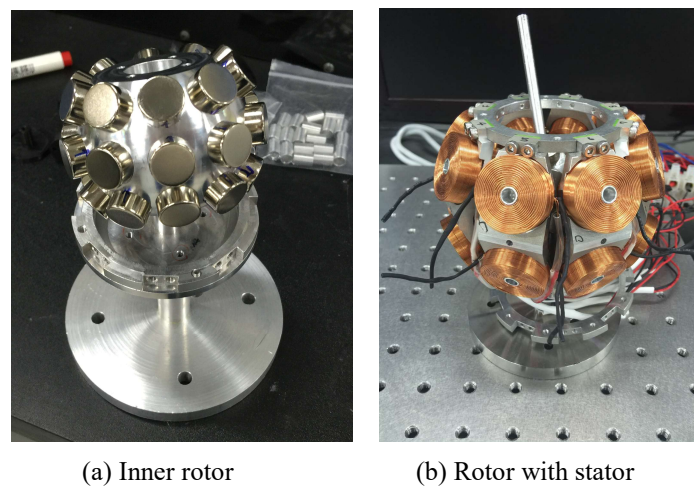

(a) Inner rotor　　　　　　(b) Rotor with stator

Fig. 5.1.2 the SWM set-ups for experiment

The pictures in **Fig 5.1.3** are taken along with three projection angles; XY, ZX, and YZ planes. The states are zero polar angle and zero azimuthal angle. As shown in **Fig 5.1.3 (a)**, the angle gauge is attached on the upper stator ring. The angle increased clockwise, but in the case of the actual z-directional rotation, the angle increased counter-clockwise.
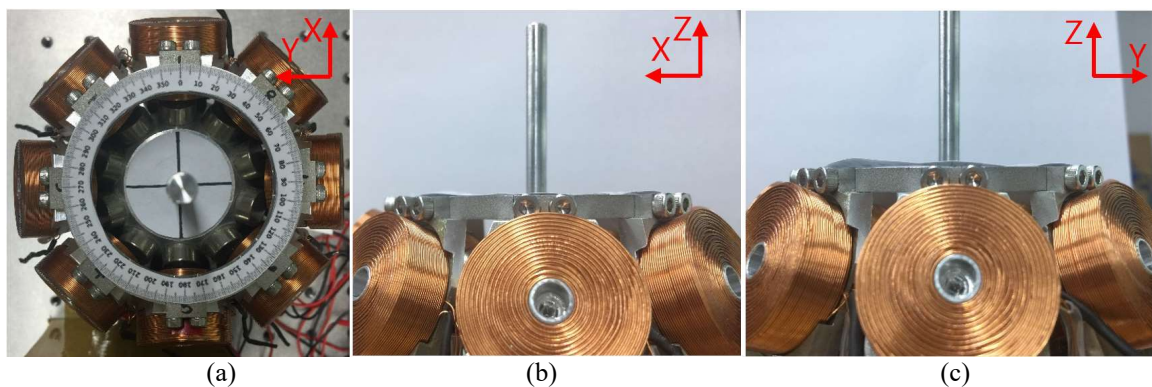

(a)　　　　　　　　　(b)　　　　　　　　　(c)

Fig. 5.1.3 three angles pictures (a) top-view; *XY*-plane projection view (b) 1ˢᵗ side view; *XZ*-plane projection view (c) 2ⁿᵈ side view; *ZY*-plane projection view.

Second, the Lab-view with MATLAB software is used for the experiments. **Fig 5.1.4** shows the control screen. There are eight current displays and three rotary switches with the up and small and triangular down buttons which have numerical value windows on the right side. The current display shows the current of each coil. The torque size controller controls the holding torque size. "alp" means the polar angle and "bet" means the azimuthal angle. The values of the rotary switches can be changed continuously. On the other hand, the values of the up and down switch buttons can be changed discontinuously; the value of torque size increase or decrease by 5N/mm and the value of alp and bet increase or decrease by 0.1 degree. Using this control panel, the SWM is controlled.
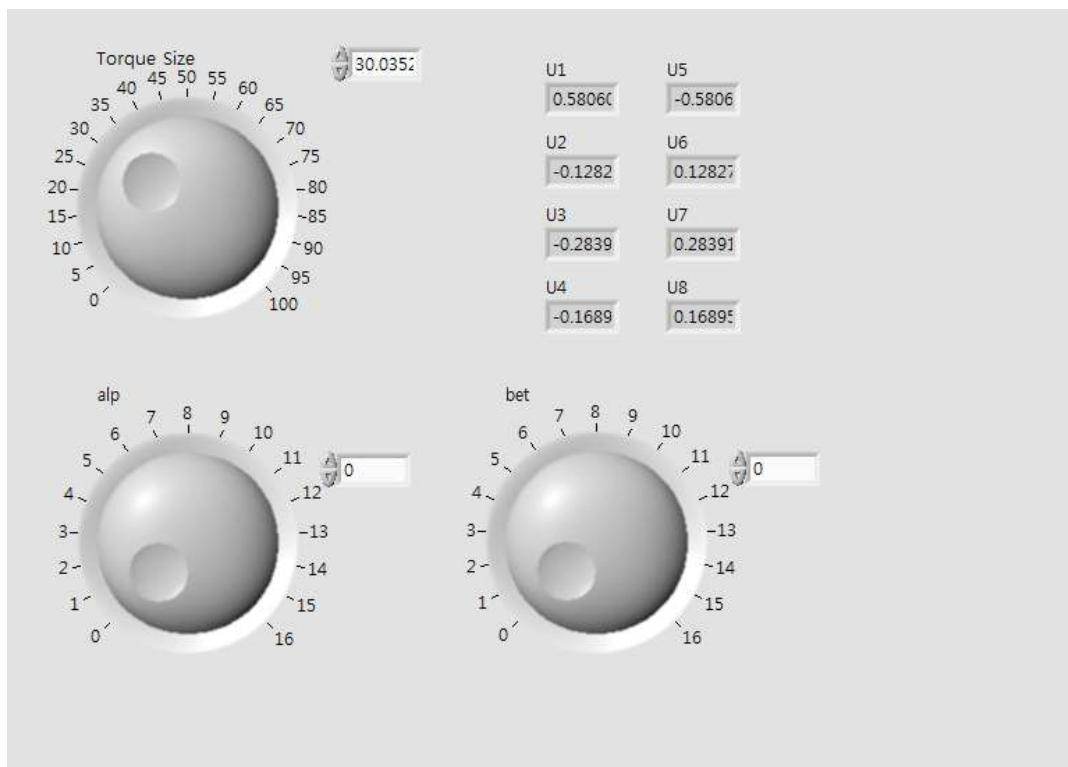

Fig. 5.1.4 Control screen in LabView

5.2 Experiment Result and Discussion

The experiment is progressed based on the set-up which is mentioned in the previous section. Three types of experiment results are shown in this section. The first case and second case are when only one directional position angle is changed; one of them is azimuthal angle and the other is polar angle changed. Third case is the combination of changing both polar and azimuthal angles.

Results of the first case are shown in **Fig 5.2.1** that only azimuthal angle is changed from 0° to 10° with two degree interval. The red lines are the reference line of X and Y axis line in absolute coordinate system and the blue lines indicate the cross mark at the rotor. To show the result, the top-view is used because the polar angle remained almost constant though there is a little change. The results show that the blue lines gradually increased and the changes are proportional to the input desired angle. For the more accurate analysis, the separation angle of the lines are measured for each case. The separation angles between the red line and the blue line are 3°, 6°, 8°, 11°, and 13° in each cases.

| (a) 0° | (b) 2° | (c) 4° |

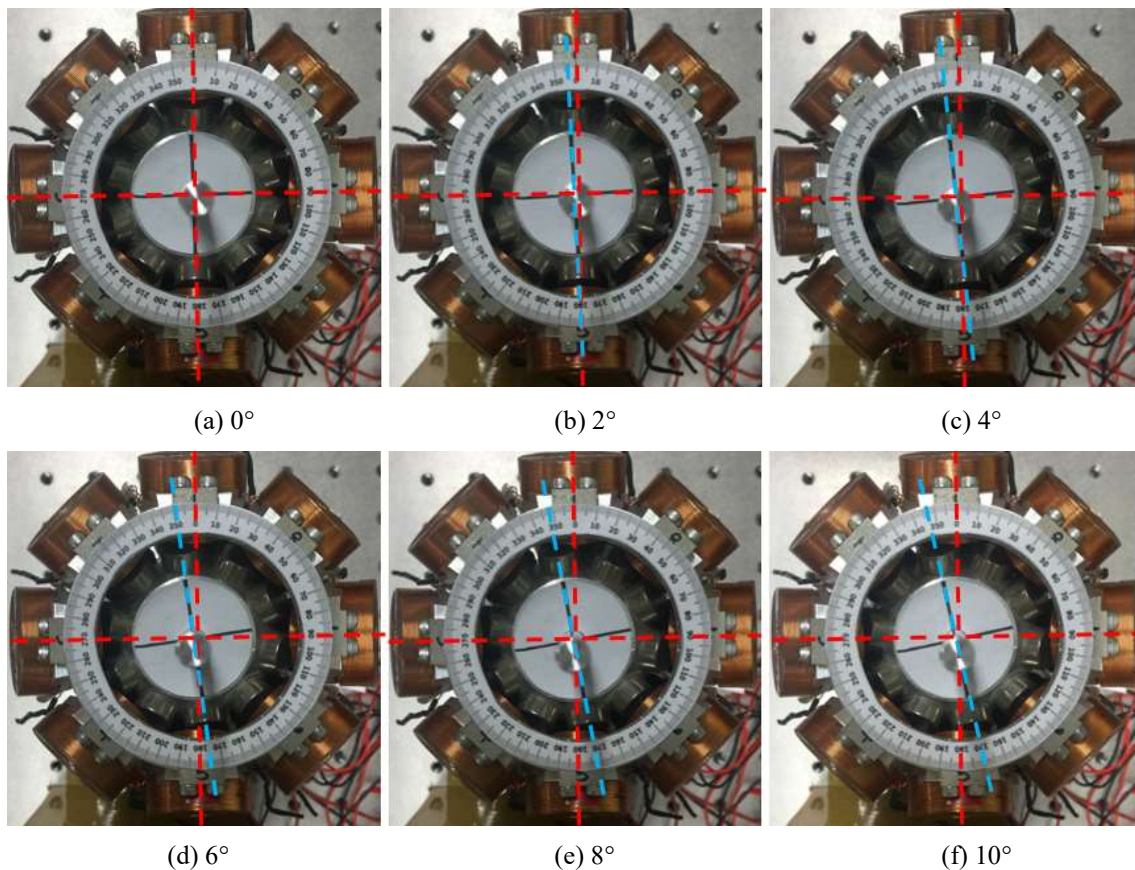| (d) 6° | (e) 8° | (f) 10° |

Fig. 5.2.1 Experiment results with changing the azimuthal angles

The results of the second case are shown in **Fig 5.2.2** with change in polar angles from 0° to 6° with two degree intervals. The results are shown with three different views. For **Fig 5.2.2 (a), (d), (g), and (j)**, the red lines are the reference line of X and Y axis in absolute coordinate system. For the rest, the red lines are the reference line of Z axis in absolute coordinate system. The blue lines are drawn along with the shaft of the rotor. Each cases are separated by rows. **Fig 5.2.2 (a) to (c)** are the home-position state. **Fig 5.2.2 (d) to (f)** are when the polar angle is changed by 2°. **Fig 5.2.2 (g) to (i)** are when the polar angle is changed by 4°. **Fig 5.2.2 (j) to (l)** are when the polar angle is changed by 6°. According to them, it is observed that the first and third column images did not show any deviation from the reference lines. For the second column, the separation angles between blue lines and reference lines are measured. The measured separation angle values are 3°, 5° and 7°.

The results of the first experiment and the second experiment show that the measured values of the separation angle are generally changed in proportional to the desired angles, considering that they are open-loop controls without the external torque due to gravity.
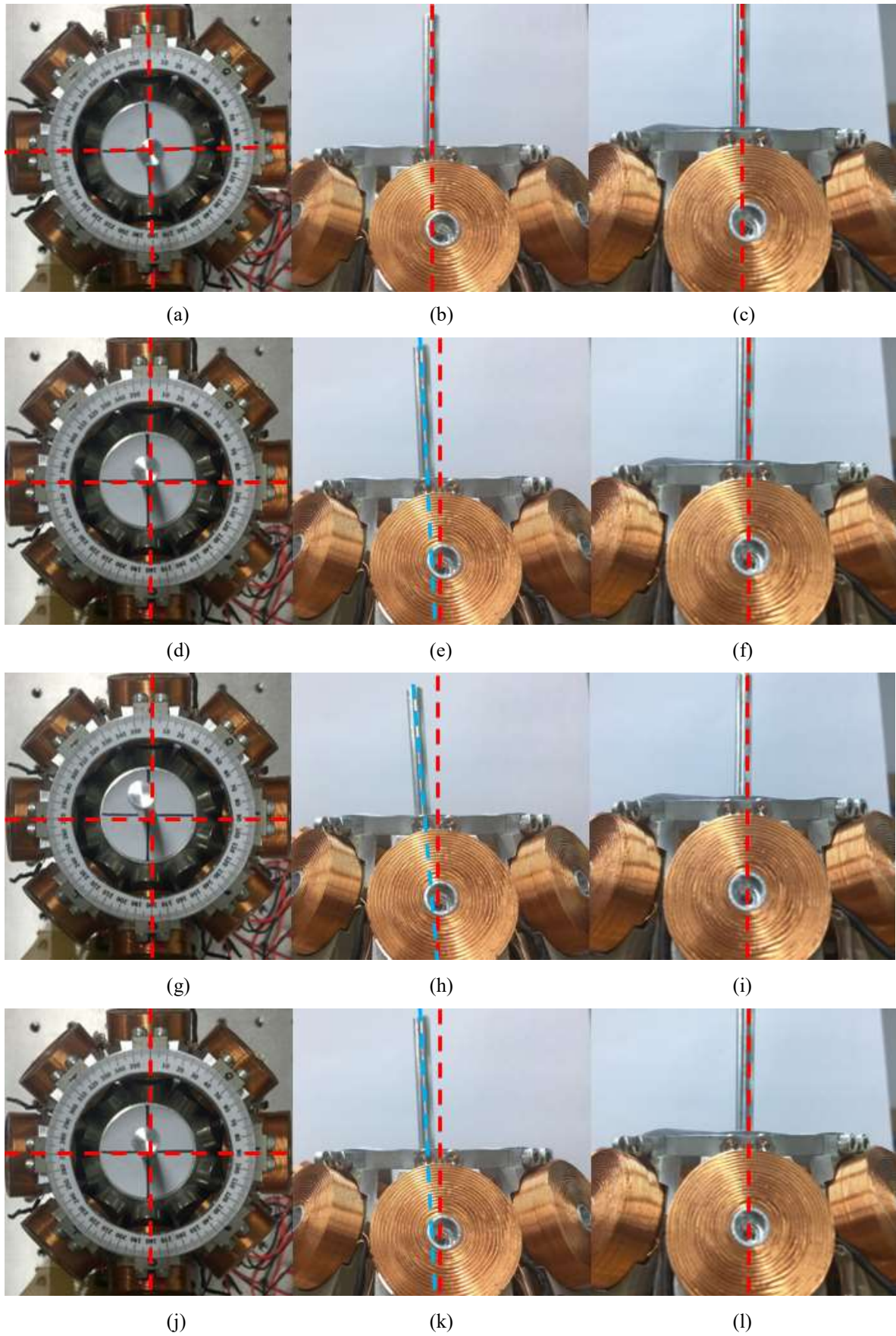
(a) (b) (c)

(d) (e) (f)

(g) (h) (i)

(j) (k) (l)

Fig. 5.2.2 Experiment results with changing polar angles

The third case of experiment is randomly chosen. The **Fig 5.2.3** shows the results when the desired polar angle is 2° and the azimuthal angle is 10°. The direction of angles follows the desired angle,. The values of separation angles from the home-position are 11° in the first figure, 3° in the second figure, and 0.5° in the third figure. Similarly, the **Fig 5.2.4** shows the results when the desired polar angle is 4° and the azimuthal angle is 4°. The values of separation angles from the home-position are 5° in the first picture, 4° in the second picture, and 1.5° in the third picture.
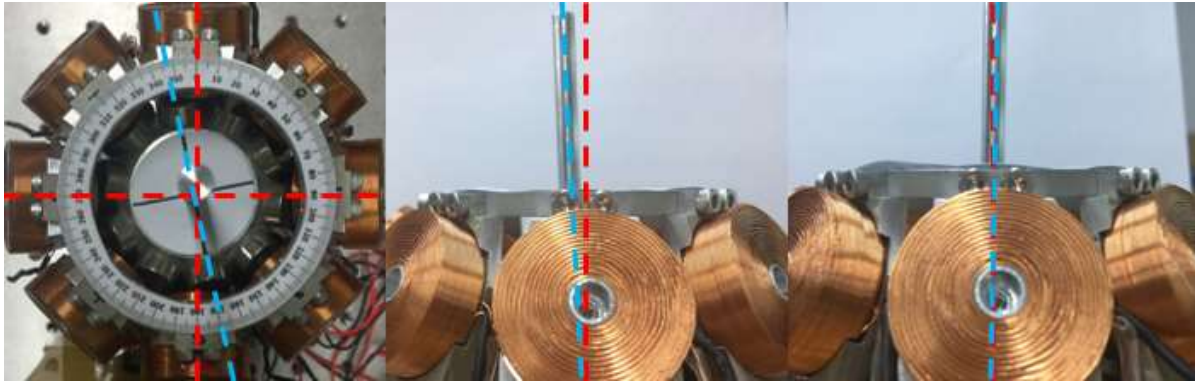

Fig 5.2.3The polar angle is 2 degrees and the azimuthal angle is 10 degrees.
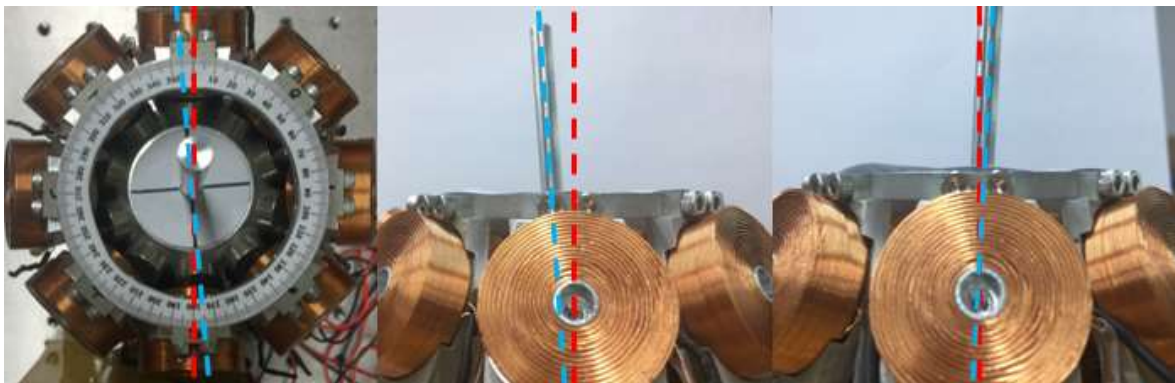

Fig 5.2.4 The polar angle is 4 degrees and the azimuthal angle is 4 degrees.

To verify the suitability of the simplified torque model, the experiments are proceeded with various desired angles. Also, the experiments are proceeded with increasing the motion by 0.1° from the home-position to desired position as well as steady state in the desired positions. In this process, disturbance occurred when the movements are changed. In addition, sudden position change occurs when the polar angle approached 6°. This phenomenon may be caused by the existence of various equilibrium points in the same current state due to many poles in the PM of the stator. Also, the inaccurate control is observed when the EM is located at the boundary of sections. This error may be because of unit-cross product term approximation.

VI. Conclusion.

The magnetic field analysis is indispensable for controlling SWM. In the previous studies, the calculation time required for torque modeling through magnetic field analysis was quite long, which made it difficult to be applied to the real-time control. During this work, the torque modeling is simplified with assumptions; the magnetic circuit is linear, the 4EMs-1PM model from the structural restriction, the cross product term can be ignored when it only has perpendicular and radial directional torque. The torque generated by six PMs which are lined with two columns and one EM is compared with results done by simplified torque modeling and the other simulation tools. As a result, it is found that the simplified torque modeling shows the fastest simulation results with similar trend to other simulation tools. Then, the results are confirmed through experiments. After the suitability of the simplified torque model is verified, it is applied to actual SWM design. Then the torque matrix can be determined which are the linear relation between current and torque. With this matrix, the position is controlled according to the push-pull principle. The experimental results show that the output is similar to the desired input considering that it is an open-loop control and excluded external torque acting as gravity. However, the disturbance occurs in non-continuous-angle-inputs in the course of experiment, and among them the unstable cases also occur. For the further study, if there is a modification to the angle part, which is a singular point that the current direction of EM changes, the simplified torque model would be enough to be applied to the actual SWM.

Reference

[1] Lee, K-M. & C.-K. Kwan, 1991, *"Design Concept Development of a Spherical Stepper for Robotic Applications,"* IEEE T-Robotics and Automation, Vol. 7, no.1, pp. 175-180, February 1.

[2] Vachtesevanos, G.J., K. Davey, & K.M. Lee, 1987, "Development of a Novel Intelligent Robotic Manipulator," IEEE Control Systems Magazine, June.

[3] Foggia, A., E. Oliver & F. Chappuis , 1988, "New Three DOF Electromagnetic Actuator," Conference Record – IAS Annual Meeting, Vol. 35, New York.

[4] Hollis, R.L., A.P. Allan, & S. Salcudean, 1987, "A Six Degree-of-freedom Magnetically Levitated Variable Compliance   Fine Motion Wrist," Fourth Int'l Symp. on Robotics Research, Santa Cruz.

[5] Kaneko, K., I. Yamada, &   K. Itao,   1988,   "A Spherical DC Servo Motor with Three Degrees of Freedom," ASM Dyn.   Sys.   & Con. Div., Vol. 11, p. 433.

[6]   Neto, L., R. Mendes, & D. A. Andrade, 1995, "Spherical Motor- a 3D Position Servo," Proc. IEEE Conf. on Electrical Machines and Drives, 11-13 Sept., pp. 227-231

[7] Lee, K-M., R. Roth, and Z. Zhou, 1996, "Dynamic Modeling and Control of a Ball-joint-like VR Spherical Motor," ASME J. of Dyn. Sys. Meas. and Control, vol. 118, no. 1, pp. 29-40, March.

[8] Chirikjian, G. S., & D. Stein, 1999, "Kinematic Design and Commutation of a Spherical Stepper Motor," IEEE/ASME T-Mechatronics Vol. 4, No. 4, Dec.

[9] Wang, J., G. Jewel, & D Howe, 2003, "Design and Control of a Novel Spherical Permanent Magnet Actuator with Three DOF," IEEE/ASME Trans. on Mechatronics, Vol. 8, No. 4, Dec., 457-467.

[10] Shigeki, T., Osamu, M., & Guoqiang, Z., 1996 "Development of New Generation Spherical Ultrasonic Motor," ICRA96, pp. 2871-2876.

[11] Lee, K.-M. , H. Son, and J. Joni, "Concept Development and Design of a Spherical Wheel Motor (SWM)," IEEE ICRA 2005, April 18-22, 2005, Barcelona, Spain.

[12] Lee, K.-M. , and H. Son, "Torque Model for Design and Control of a Spherical Wheel Motor"

IEEE/ASME, July 24-28, 2005, California, USA.

[13] H. Son and K.-M. Lee, "Distributed multipole models for design and control of PM actuators and sensors," IEEE/ASME Trans. Mechatronics, vol. 13, no. 2, pp. 228–238, 2008.

[14] F. Wu, J. Jeon, S. K. Moon, H.-J. Choi, and H. Son, "Voice Coil Navigation Sensor for Flexible Silicone Intubation," IEEE/ASME Trans. Mechatronics, vol. 21, no. 2, pp. 851–859, 2016.

[15] F. Wu, S. K. Moon, and H. Son, "Orientation measurement based on magnetic inductance by the extended distributed multi-pole model," Sensors, vol. 14, no. 7, pp. 11504–11521, 2014.

Acknowledgements

First of all, I would like to express my gratitude and respect to my advisor Professor Dr. Hungsun Son. Especially, it was great honor to have been able to conduct research on SWM, the subject of his research. During this study, I was able to develop various thought while studying according to his previous research, and I was able to produce good results based on this. I am honored that I could study under Dr. Hungsun Son.

I would also like to express my thanks to Professor Dr. Joonbum Bae and Professor Dr. Gunho Kim who gave a great support to complete this study. Their advice allowed me to fill the shortcomings, without these advice it would have been hard to finish the study.

Also, I would like to thank my laboratory members and my precious friends. There sincere advices were always helpful and supportive.

I would express a deep sense of gratitude to my family for their understanding and support. I would not be here without them.

Last but definitely not least, I would also thank to people who I did not mentioned the name, yet were a great support to me in my process of learning.